Chapter

MODELING OF RECRYSTALLIZATION OF COMMERCIAL PARTICLE CONTAINING AL-ALLOYS

Knut Marthinsen[1,*], Ke Huang[2] and Ning Wang[3,†]

[1]Department of Materials Science and Engineering,
Norwegian University of Science and Technology (NTNU),
Trondheim, Norway
[2]State Key Laboratory for Manufacturing System Engineering,
Xi'an Jiaotong University, PR China
[3]Gränges Technology AB, Finspång, Sweden

ABSTRACT

In order to describe and discuss the recrystallization behavior of commercial particle containing Al-alloys, the physical basis and a mathematical formulation of a softening model nicknamed *ALSOFT*, accounting for the combined effect of recovery and recrystallization

* Corresponding Author Email: knut.marthinsen@ntnu.no.
† Email: ning.wang@granges.com.

behavior during annealing of heavily deformed aluminum alloys have been reviewed. The prediction power of the model is discussed using two different Al-Mn-Fe-Si-alloys experiencing different processing conditions, giving very different microchemistries in terms of solute and second-phase particle structures. The experiments clearly demonstrate the strong influence of microchemistries and in particular the strong dispersoid effects that may be experienced during back-annealing, either from pre-existing dispersoids or concurrent precipitation. It is demonstrated that good model predictions may be obtained for alloys and conditions which are not or to a limited extent influenced by particle drag effects and concurrent precipitation while conditions strongly affected by these effects are increasingly difficult to model and in the most extreme cases impossible with reasonable input model parameters. Possible causes for these difficulties are discussed and potential improvements of the model are suggested.

Keywords: recovery, recrystallization, concurrent precipitation, Zener drag, modeling

INTRODUCTION

Thermo-mechanical processing of aluminum alloys is commonly characterized by a complex sequence of deformation (hot/cold) and annealing steps, to achieve the final microstructure, which largely determines the properties and performance of the final material and/or product. E.g., during sheet rolling the material is first hot-rolled, and then cold rolled before final annealing. When the cold deformed material is annealed at a sufficient high temperature, recrystallization will take place, driven by the stored energy (mainly in the form of line defects, i.e., dislocations) introduced during deformation. Recrystallization refers the formation ("nucleation") of new dislocation-free grains and the gradual consumption of the cold worked matrix by growth of these grains (by migration of high-angle grain boundaries). The process of recrystallization of plastically deformed metals and alloys is of central importance during thermomechanical processing for two main reasons. The first is to soften and restore the ductility of material hardened by deformation. The second is to

control the grain structure and texture (grain orientation distribution) of the final product. For aluminum alloys, recrystallization after deformation is the only method for producing a completely new grain structure with a modified grain size, shape, and, in particular, a desired grain orientation distribution (texture), all aspects of which are crucial for the properties of the semi-finished material (rolled sheet). In some cases, a partly back-annealed (softened/recrystallized) condition is desired, to balance hardness and ductility. In such cases, it is crucial being able to control the softening kinetics.

Most commercial aluminum alloys have a complex microchemistry in the form of solid solution levels of alloying elements, volume fraction and size of constituents and dispersoids, and, which may be strongly modified during thermomechanical processing. Although the type and amount of solutes may play a role (through solute drag effects), the most significant effects are related to the second phase particles, which may strongly affect both nucleation and growth of recrystallized grains, and thus both the kinetics and the final grain structure and texture. In which way the second phase particles will affect the recrystallization behavior of a given alloy, as compared to a single-phase alloy, will depend on whether they are present prior to deformation or are precipitated during/after recrystallization. If present before the deformation stage, to which extent and how the recrystallization process will be influenced, will depend on the type, size and spatial distribution of the particles, through their influence on the deformed state, and the subsequent nucleation and growth behavior. Large particles will generally accelerate the reaction, through particle stimulated nucleation (PSN) of recrystallization and strongly influence the final grain size and texture (Nes and Embury 1975, Daaland and Nes 1996). On the other hand, a high density of small particles (dispersoids) will generally give rise to a significant drag force (Zener pinning), acting on moving sub-grain and grain boundaries (of growing recrystallization grains) and may strongly retard, and in some cases completely suppress recrystallization and strongly modify the final grain structure and texture. This influence may be even more pronounced in case of precipitation simultaneous with the recrystallization reaction (i.e., concurrent precipitation) (Nes and Embury 1975, Daaland and

Nes 1996, Vatne, Engler et al. 1997, Humphreys and Hatherly 2004, Sjolstad, Marthinsen et al. 2004, Tangen, Sjolstad et al. 2010).

In the present chapter all these aspects will be covered, i.e., the effects of solute and in particular the effects of second phase particles on the *nucleation and growth kinetics* of recrystallization as well as the effects on *final grain structure*. The different phenomena and reactions will be described and discussed in terms of classical theories and simple models (when available), and exemplified by experiments and numerical simulations. A special attention will be given to recent findings in AlMn-alloys, which perfectly illustrate the potential strong effects of second-phase particles on the softening behavior, in particular the influence of pre-existing dispersoids and/or concurrent precipitation, leading to strongly suppressed nucleation, sluggish growth and a recrystallized grain structure of coarse elongated grains and partly unconventional textures.

As basis for describing and illustrating the influence of different microchemistries, in terms of solute levels, constituents and dispersoids will make use of the so-called *ALSOFT* mode. The *ALSOFT* model is a statistical mean field model for the simulation of the softening behavior of deformed Al-alloys that was developed within the Norwegian aluminum community in the nineties (Vatne, Furu et al. 1996, Vatne, Marthinsen et al. 1996, Saeter 1998). The model accounts for the combined effect of static recovery and recrystallization during annealing of the deformed state and incorporates the effects of solutes (solute drag), constituents (PSN) and dispersoids (Zener drag), by the use of classical models for these phenomena. Although not the most sophisticated model that exists, it still mainly reflects our current understanding and model descriptions for these phenomena, and is well suited to illustrate the effects of solute and in particular second phase particles on the recovery and recrystallization behavior. The model has successfully been applied to predict the softening behavior of various Al-alloys, in particular after hot deformation and conditions of mainly isothermal annealing [(Vatne, Furu et al. 1996, Vatne, Marthinsen et al. 1996, Saeter 1998, Marthinsen, Abtahi et al. 2004, Engler, Lochte et al. 2007, Marthinsen, Friis et al. 2012).

The structure of the chapter will be as follows. Firstly, a rather detailed presentation of the *ALSOFT* model will be given, including some recent modifications, which are assumed to be relevant for commercial Al-alloys with a complex microchemistry. Generic model predictions will then be presented, which illustrate how the recovery and recrystallization behavior depend on processing conditions and alloy microchemistry. These generic model results will then be followed by a case study where the *ALSOFT* model is applied and its prediction power discussed in relation to a recent comprehensive experimental study for the back-annealing behavior of selected Al-Mn-Fe-Si–alloys with various microchemistries presented in a series of papers by the present authors (Huang, Wang et al. 2014, Huang, Engler et al. 2015, Huang, Li et al. 2015, Huang, Li et al. 2015, Huang and Marthinsen 2015, Huang, Loge et al. 2016, Wang, Huang et al. 2016, Huang, Zhang et al. 2017). These experimental studies have clearly shown that the softening behavior during back annealing of cold rolled Al-Mn(-Fe-Si) alloys is the result of a critical balance between the processing conditions and microchemistry and its associated changes during processing, in terms of size and number of constituents, solute level of alloying elements and in particular the presence of dispersoids. In particular, it has been shown that finely dispersed dispersoids, whether pre-existing or precipitated concurrently with the recovery and recrystallization reaction, may strongly retard the softening kinetics and give a coarse and uneven grain structure.

In view of the ability of the *ALSOFT* model to capture these phenomena and to reproduce the characteristics of these experiments, the chapter will end with a critical review and discussion of our current understanding, and models for the recovery and recrystallization behaviour in commercial Al-alloys, and suggest some ideas for modifications that might be adequate and necessary to handle cases/conditions where current model(s) are not satisfactory.

MODELING RECOVERY AND RECRYSTALLIZATION IN PARTICLE CONTAINING AL-ALLOYS

The *ALSOFT* Model

The main concepts and mathematical implementation of the *ALSOFT* model is well documented in the literature (Vatne, Furu et al. 1996, Vatne, Marthinsen et al. 1996, Saeter 1998, Engler, Lochte et al. 2007); however for completeness and as basis for discussing already implemented and possible further extensions of the model, the main ingredients will be also be presented here.

The *ALSOFT* model is based on a two-parameter description of the as-deformed sub-structure after cold/hot deformation where the microstructure is characterized by an average sub-grain size, δ, and a dislocation density, ρ_i, inside the sub-grains. The average sub-grain size after deformation can be obtained from experiments or from adequate models, like the ALFLOW model, e.g., (Nes 1997, Marthinsen and Nes 2001, Nes and Marthinsen 2002). For hot deformation, the following empirical relationship between the subgrain size and the Zener-Hollomon parameter has been found to be adequate (Nes 1995):

$$\frac{1}{\delta} = \frac{RT}{A} \ln\left(\left(\frac{Z\delta^2}{B}\right)\right) \tag{1}$$

where A and B are alloy-dependent constants, and Z is the Zener-Hollomon parameter, $Z = \dot{\varepsilon}\ exp[Q/RT]$. Here Q is an activation energy and R is the universal gas constant. The sub-grain size δ and the dislocation density ρ_i are in this case linked through the scaling relationship $\rho_i = \left(C/\delta\right)^2$, where C is a constant ~2.

During annealing of the as-deformed state recovery will take place through sub-grain growth and by annihilation of the sub-grain interior

dislocations. In the original version of the *ALSOFT* model, recovery kinetics is assumed to be controlled by solute drag, where the rate controlling mechanism is assumed to be thermal activation of solute atoms away from climbing jogs. Based on this assumption the following explicit evolution equations with time for sub-grain size and dislocation density, respectively, have been derived (Nes 1995, Saeter 1998, Engler, Lochte et al. 2007):

$$\frac{d\rho_i(t)}{dt} = -v_D b A_\rho B_\rho \rho_i(t)^{3/2} \exp\left(-\frac{U_a}{RT(t)}\right) 2\sinh\left(\frac{A_\rho G b^4 \sqrt{\rho_i(t)}}{kT(t)}\right) \qquad (2)$$

$$A_\rho = w_\rho \left(c_{ss}^{eff}\right)^{-e}$$

$$\frac{d\delta(t)}{dt} = v_D b A_\delta B_\delta \exp\left(-\frac{U_a}{RT(t)}\right) 2\sinh\left(\frac{A_\delta G b^4}{kT(t)}\frac{1}{\delta(t)}\right); A_\delta = w_\delta \left(c_{ss}^{eff}\right)^{-e} \qquad (3)$$

Here G is the shear modulus, b is Burgers vector (b = 0.286 nm in aluminum), γ_{SB} is the sub-boundary energy, v_D is the Debye frequency, k is Boltzmann's constant, $w_{\rho,\delta}$ *and* $e_{\rho,\delta}$ are model parameters, and $B_{\rho,\delta}$ alloy specific fitting constants. c_{ss}^{eff} is an effective level of solute (at%) derived from a summation of the solute concentration of the individual alloy elements, weighted with their activation energy for diffusion. U_a is an activation energy, which in the case of solute drag equals that of diffusion of the relevant solutes.

The instantaneous stored energy/driving pressure for recrystallization due to cell interior dislocations and sub-grains is calculated according to the following equation:

$$P_D(t) = \alpha \frac{\gamma_{SB}}{\delta(t)} + \frac{1}{2} G b^2 \rho_i(t)^2 \qquad (4)$$

In this equation the subgrain boundary energy can be approximated by the Read-Shockley relation as follows (Read 1953, Humphreys and Hatherly 2004):

$$\gamma_{SB} = \frac{Gb\theta}{4\pi(1-\nu)} \ln\left(e\frac{\theta_c}{\theta}\right) \tag{5}$$

where ν is the Poisson ratio, θ is the average subgrain misorientation and θ_c is the critical value at which a sub-boundary becomes a high-angle boundary (typically taken to be ~15°). α is a constant of the order of three.

In the presence of finely dispersed dispersoids a dragging pressure, i.e., a Zener pressure $P_Z(t)$ will result. With dispersoids of average size, $r_p(t)$, and a volume fraction of, $f_p(t)$, (both which may change with time due to precipitation) the classical Zener pressure expression is given by (Nes, Ryum et al. 1985, Humphreys and Hatherly 2004):

$$P_Z(t) = \frac{3}{2}\frac{f_p(t)\gamma_{GB}}{r_p(t)} \tag{6}$$

and the driving pressure for recrystallization has to be modified accordingly, i.e., giving an effective driving pressure $P_D^{eff}(t)$:

$$P_D^{eff}(t) = P_D(t) - P_Z(t) \tag{7}$$

In this case, with a Zener pressure from dispersoids, the equation for sub-grain growth has in the present work also been modified accordingly, i.e., in analogy with normal grain growth, the driving pressure resulting from curvature is reduced by the Zener drag and the following equation is obtained:

$$\frac{d\delta}{dt} = \nu_D b A_\delta B_\delta \cdot \exp\left(-\frac{U_g}{RT(t)}\right) \cdot 2\sinh\left(\frac{A_\delta}{kT(t)}\left(\frac{Gb^4}{\delta(t)} - P_Z(t)\frac{b^3}{\alpha_4\delta(t)}\right)\right) \quad (8)$$

the consequences of which will be discussed later in this paper.

The recrystallization module of *ALSOFT* is an extension of the classical Johnson-Mehl-Kolmogorov-Avrami (*JMAK*) approach, treating recrystallization as a nucleation and growth process (Kolmogorov 1937, Avrami 1939, Johnson 1939, Avrami 1940, Avrami 1941). Nucleation of recrystallization is assumed to take place from sub-grains, which fulfill the general nucleation criteria for recrystallization, i.e., sub-grains that fulfil the Gibb's Thomson relationship:

$$\delta^*(t) > \frac{4\gamma_{GB}}{P_D(t) - P_Z(t)} \quad (9)$$

and which moreover are surrounded by high-angle boundaries, i.e., at deformation heterogeneities in the material where this is the case.

In the current version of *ALSOFT*, three types of nucleation sites are considered, i.e., nucleation from deformation zones around large particles (*PSN*), nucleation from old grain boundaries and nucleation from retained cube bands (Daaland and Nes 1996, Vatne, Furu et al. 1996). The total density of nucleation sites is given by

$$N_{Tot} = N_C + N_{GB} + N_{PSN} \quad (10)$$

The density of PSN sites, N_{PSN}, is determined by an integration of the particle size distribution $f(\eta)$:

$$N_{PSN} = C_{PSN} \int_{\eta^*}^{\infty} f(\eta) d\eta \quad (11)$$

where the particle size distribution is characterized through the distribution parameters N_0 and L, i.e.,

$$f(\eta) = N_0 L \exp(-L\eta) \tag{12}$$

where C_{PSN} is a constant which determines the number of recrystallized grains nucleated at each particle that is larger than η^*. η^* is a critical particle size for a successful nucleation of a grain (assumed to scale with δ^* (Eq. 9)) that can be derived from the Gibbs-Thompson equation, i.e., $\eta^*=4\gamma_{GB}/(P_D-P_Z)$, where γ_{GB} is the specific grain boundary energy between the nucleus and the deformation matrix. The following relationship results for the nucleation of PSN nuclei:

$$N_{PSN} = C_{PSN} N_0 \exp\left(-\frac{4\gamma_{GB} L}{P_D - P_Z}\right) \tag{13}$$

The density of cube sites, Nc, is given by

$$N_C = C_C \bar{\delta}_C A(\varepsilon)(1-R_C) R_S S_C^* \text{ (14).} \tag{14}$$

Here $\bar{\delta}_C$ is the average size of the cube subgrains, with $\bar{\delta}_C \approx 1.3 \cdot \bar{\delta}_{matrix}$, $A(\varepsilon)$ is the surface area per unit volume of cube grains that have undergone a deformation of an effective strain ε, R_S is the fraction of cube bands surrounded by the S deformation texture component and S_c^* is the density of over-critically large subgrains within the cube bands. $A(\varepsilon)$ is given by the initial grain size D_0 and the instantaneous volume fraction of cube in the material, $R_c = f(\varepsilon,Z)$. The factor $(1-R_C)$ is included because a cube band with another cube grain as neighbor will not provide nuclei and C_C is a constant (Vatne, Furu et al. 1996).

In analogy with Eq. (14) the density of grain boundary nuclei becomes:

$$N_{GB}=2C_{GB}\,\bar{\delta}_{matrix}(1-R_C)S^{*}_{GB}A(\varepsilon) \tag{15}$$

where the different terms have the same/corresponding meaning as above and C_{GB} is a (fitting) constant.

The recrystallization kinetics is calculated by applying the standard assumptions of site saturation nucleation kinetics and a random distribution of nucleation sites, i.e., the following transformation kinetics equation is obtained:

$$\frac{dX(t)}{dt}=\left(1-X(t)\right)N_{Tot}\,4\pi\cdot\left(r(t)\right)^{2}\cdot G(t) \tag{16}$$

Here *X(t)* is the fraction recrystallized after an annealing time *t*, *r(t)* is the size and *G(t)* the growth rate of the recrystallized nuclei/grain. These two quantities are linked through the following relationship:

$$\frac{dr}{dt}=G(t) \tag{17}$$

where growth rate is generally given by

$$G(t)=M(t)\cdot\left(P_D(t)-P_Z(t)\right) \tag{18}$$

Here *M(t)* is the boundary mobility (assumed to be orientation independent) which depend on the temperature through the following Arrhenius type relation:

$$M(t)=\frac{M_0}{c_{ss}^{eff}kT}\exp\left(-\frac{U_{RX}}{RT}\right) \tag{19}$$

Here U_{RX} is an activation energy for migration of high-angle grain boundaries, most likely determined by slow diffusing elements like *Mn*. The

effect of solute drag is included through the inverse proportionality to c_{ss}^{eff}, a dependency consistent with the high solute limit of the classical Cahn-Lücke-Stüwe approach (Cahn 1962, Lucke and Stuwe 1971). In the case of a multicomponent alloy, the total concentration of solutes, c_{ss}^{eff}, is derived from summation of the solute concentration of the individual alloy elements, weighted by their activation energy for diffusion of the solutes (Vatne 1999).

Once the fraction recrystallized is determined, the grain size in the transformed regions can then easily be calculated as:

$$D = (X / N_{Tot})^{1/3} \tag{20}$$

where N_{Tot} is the total number of nuclei (Eq. 10), while the fractions of the different recrystallization texture components are given as $f_i = N_i/N_{Tot}$.

The assumption of site-saturation nucleation kinetics has partly been introduced for mathematical convenience, but it has also been shown to be an adequate assumption for aluminum for recrystallization following hot deformation (Daaland and Nes 1996, Alvi 2005, Alvi, Cheong et al. 2008). However, it is a question whether this assumption still holds for recrystallization following cold deformation and more specifically during non-isothermal annealing conditions. This aspect will be discussed later in the chapter.

Because of the combined reactions of recovery and recrystallization, the associated yield stress (YS) during back-annealing is then given by the following relationship (Saeter 1998, Marthinsen, Abtahi et al. 2004, Engler, Lochte et al. 2007):

$$\sigma_y(t) = \sigma_0(t) + \left[\alpha_1 MGb\sqrt{\rho_i(t)} + \alpha_2 MGb\frac{1}{\delta(t)} \right]\left(1 - X(t)\right) \tag{21}$$

where α_1 and α_2 are constants, with typically values of *0.3* and *2.5*, respectively. σ_0 is the yield stress of the fully soft condition and may be expressed through

$$\sigma_o(t) = \sigma_i + \sigma_{ss}(t) + \sigma_p(t) \tag{22}$$

where $\sigma_{ss}(t)$ is the strength contribution from atoms in solid solution:

$$c_{ss}(t) = k\left(c_{ss}^0 + c_{ss}^{eff}(t)\right)^{1/2} \tag{23}$$

Here c_{ss}^0 is a base level of solute due to impurity atoms (and/or minority solute atoms not for accounted by $\sigma_{ss}(t)$ and $\sigma_p(t)$ is the strength contribution from non-shearable particles (primary particles and/or dispersoids), i.e.:

$$\sigma_p(t) = \frac{AGbM}{1.24 \cdot 2\pi}\left[\frac{1}{\lambda}\ln\left(\frac{\lambda}{b}\right)\right]; \quad \lambda = 0.8\left(\sqrt{\frac{\pi}{f_p}} - 2\right)\cdot r_p \tag{24}$$

k is a constant that has to be fitted to the actual alloy, and A is a constant of the order of one. λ is the particle spacing (surface to surface) in the slip plane (Brown 1971, Nes and Marthinsen 2002).

Generic Model Predictions

The present work is based on a MATLAB®-implementation of *ALSOFT* where the time-temperature schedule during annealing can be explicitly specified on input, together with the corresponding time evolution of the effective solute level (Eq. 23) and the Zener drag (Eq. 6).

In order to illustrate how the model responds to different processing parameters during deformation and back-annealing as well as material parameters depending on alloy composition, initial microstructure (grain structure and texture) and microchemistry state (i.e., solid solution level,

volume fraction/number density and size/size distribution of constituents particles and dispersoids, as determined by the casting and homogenization procedure), a set of generic model simulations has been carried out with representative variations in these parameters relevant for this work and AA3xxx-alloys in general (Marthinsen, Abtahi et al. 2004, Sjolstad, Marthinsen et al. 2004). The generic model calculations also include modeling results showing how the model responds to some key model parameters that generally have to be fitted to/determined from experiments. This has been done to illustrate the sensitivity of the model to these parameters and also as a basis for discussing the actual model predictions presented in the next section where the model is used in relation to the experimental results presented in previous work (Huang, Wang et al. 2014, Huang, Engler et al. 2015, Wang, Huang et al. 2016). The effect of dispersoids, through the Zener drag effect (cf. Eq. 6), on softening kinetics and final grain size (through the effect on nucleation (Eq. 9)) is considered in some detail, including the consequences of the new recovery model which also accounts for a possible Zener drag effect during recovery.

As a reference for the model calculations given in this part, input parameters corresponding to the as cast condition of an AlMnFeSi-alloy (1wt% Mn, 0.5 wt% Fe, 0.15wt% Si; denoted C2 (cf. Table 1 below)), cold rolled to a strain of $\varepsilon = 3$, and isothermally annealed at $T = 300^{o}$C, is used (for details see (Huang, Wang et al. 2014, Huang, Engler et al. 2015, Wang, Huang et al. 2016)). This is also the processing condition used if not explicitly stated differently. A complete list of input parameters is given in Appendix (cf. the case study chapter for some more details on the choice of relevant material parameters). A large number of these parameters are kept fixed throughout the calculations presented here, partly for convenience but also since most of them is supposed to be adequate for this work as they come from previous work/applications of the *ALSOFT*-model on similar alloys and conditions, including a set of activation energies relating to boundary migration and diffusion in AlMn-alloys (Marthinsen, Abtahi et al. 2004, Sjolstad, Marthinsen et al. 2004, Engler, Lochte et al. 2007)].

The first simulation example refers to the effect of varying (iso-thermal) annealing temperature. Temperature affects both recovery kinetics (cf. Eqs.

2-3), as well as recrystallization kinetics (growth rate of recrystallized grains; Eqs. 18 and 19) as illustrated in Figure 1. At high enough temperature recrystallization takes place within a very short time and the recovery stage is almost completely suppressed. The shift in time to reach the fully soft (recrystallized) condition is primarily determined by the activation energy in Eq. 19. It should be noted though that in the present version of *ALSOFT*, with site saturation nucleation, the final grain size is not influenced by the annealing temperature, as the density of nucleation sites is determined by the as deformed condition alone (Eqs. 9-15 & 20).

The effect of deformation conditions (temperature, strain and strain rate) will manifest itself in terms of a different *as deformed* condition, i.e., a different mean sub-grain size and a different sub-grain interior dislocation density, which again determines the stored energy and driving force for the recovery kinetics and recrystallization during subsequent annealing (Eq. 4), as well as the as deformed yield strength (Eq. 21). The effect of stored energy on the recrystallization kinetics and final grain size is illustrated in Figure 2 for a limited range of sub-grain sizes relevant to this work ($\delta \sim 0.45 - 0.65$ μm). As noted, the most pronounced effect is on the initial yield stress and initial recovery rate as well as on the final grain size (60% increase). Decreasing stored energy increases the critical sub-grain size for nucleation, and makes nucleation more "difficult," i.e., the density of all three nucleation sites decreases and the final grain size becomes larger.

For a given set of processing conditions, the alloy composition and microchemistry state may also have a significant influence on the softening behavior. Figure 3 illustrates the effect of variations in effective solute content (corresponding to the range of effective solute level of Mn (at%) obtained by the different homogenizations used in paper (Huang, Wang et al. 2014, Huang, Engler et al. 2015, Huang, Li et al. 2015, Huang, Li et al. 2015, Huang and Marthinsen 2015, Huang, Loge et al. 2016, Wang, Huang et al. 2016, Huang, Zhang et al. 2017). Decreasing the effective solute level strongly influences the recovery kinetics, consistent with Eq. 2 and 3 for which solute drag is assumed to be the rate controlling mechanism. Also the recrystallization kinetics is slowed down in accordance with the inverse

proportionality of the mobility to the (effective) solute level in Eq. 19.

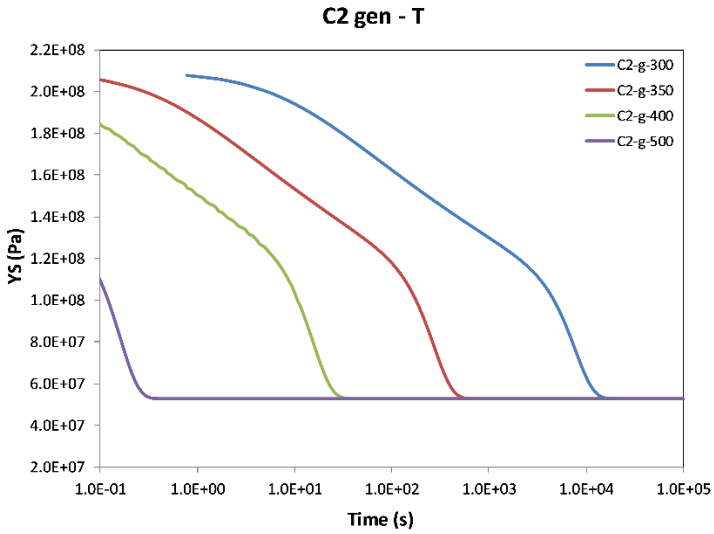

Figure 1. Generic model calculations showing the effect of different annealing temperatures on the softening behaviour of an Al-Mn-Fe-Si-alloy cold-rolled to a strain of $\varepsilon = 3$.

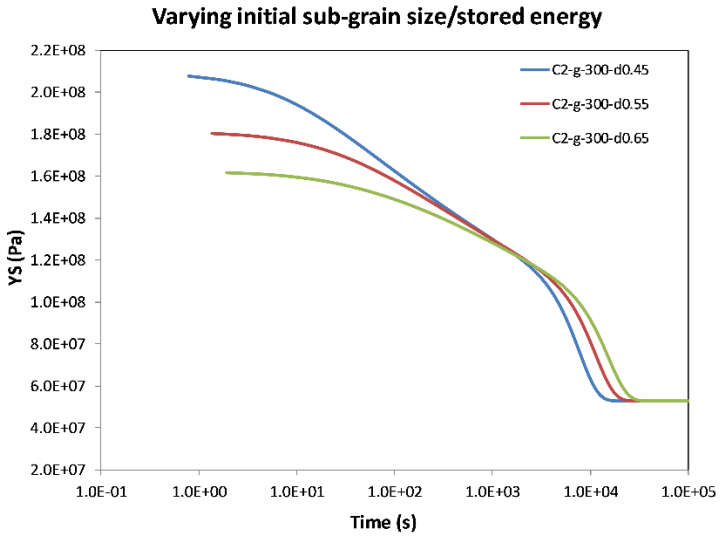

(a)

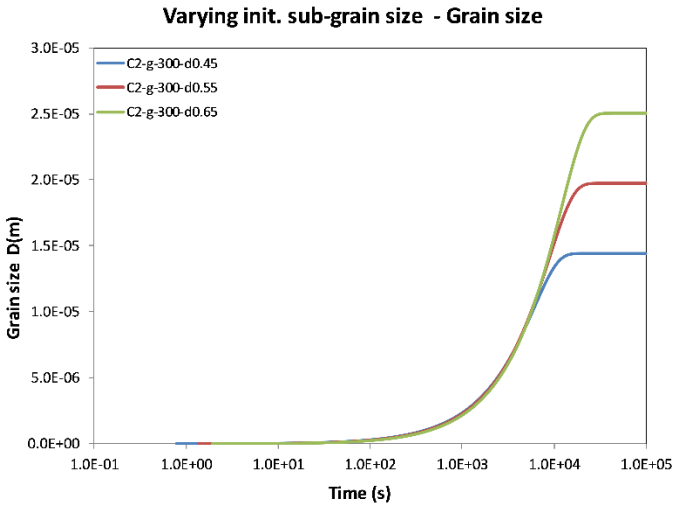

(b)

Figure 2. Generic model calculations showing the effect of differences in initial stored energy/driving force for recrystallization on the softening behavior of an Al-Mn-Fe-Si-alloy cold-rolled to a strain of $\varepsilon = 3$. (a) Kinetics. (b) Evolution in recrystallized grain size.

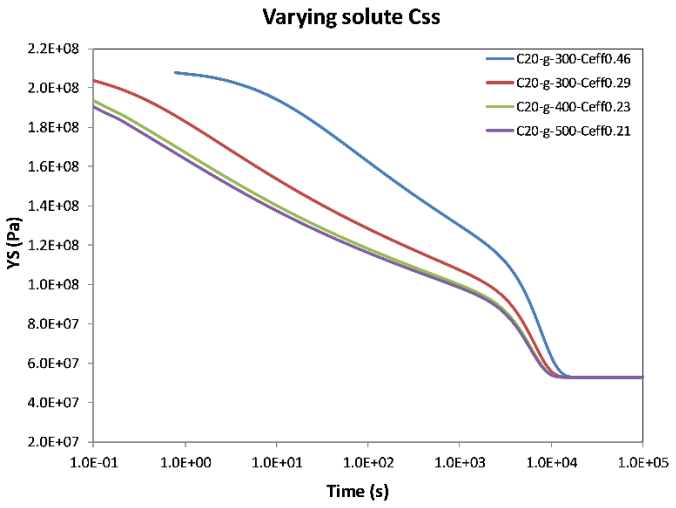

Figure 3. Generic model calculations showing the effect of different (effective) solid solution levels on the recovery and recrystallization behavior Al-Mn-Fe-Si-alloy cold-rolled to a strain of $\varepsilon = 3$.

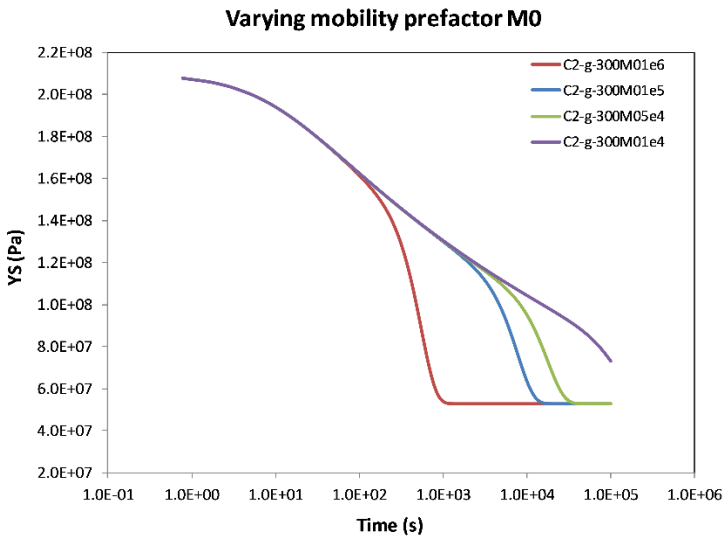

Figure 4. Generic model calculations showing the effect of differences in the mobility pre-factor M_0 on the softening behavior of an Al-Mn-Fe-Si-alloy cold-rolled to a strain of $\varepsilon = 3$.

The latter dependency is closely related to the mobility pre-factor factor M_0 (Eq. 19). This parameter is generally difficult to obtain, both theoretically and from experiments, and it is commonly taken as a fitting parameter using an initial value obtained from one or more reference experiments (for a given alloy and processing condition). As we can see from Figure 4, when M_0 changes with several orders of magnitude, the kinetics (time in seconds to recrystallized fraction) changes accordingly.

As demonstrated in (Huang, Wang et al. 2014, Huang, Engler et al. 2015, Huang, Li et al. 2015, Huang, Li et al. 2015, Huang and Marthinsen 2015, Huang, Loge et al. 2016, Wang, Huang et al. 2016, Huang, Zhang et al. 2017) the actual homogenization procedure may have a strong influence on the microchemistry state, both in terms of number density and size/size distribution of constituent particles and dispersoids where both types of particles may have a strong effect on the softening behavior.

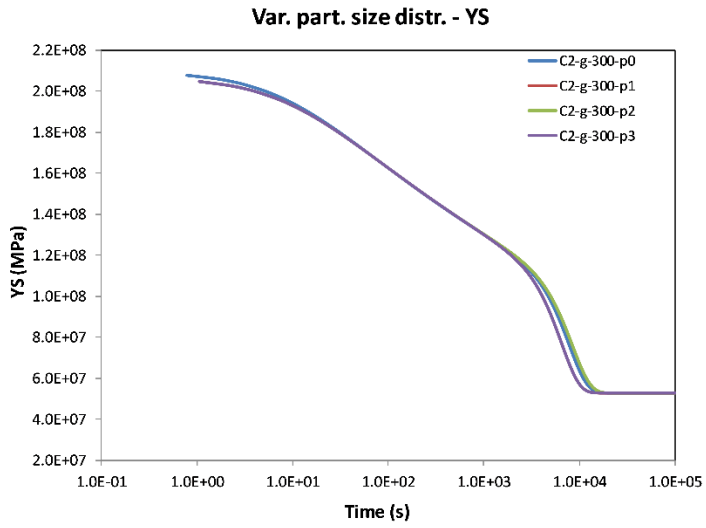

(a)

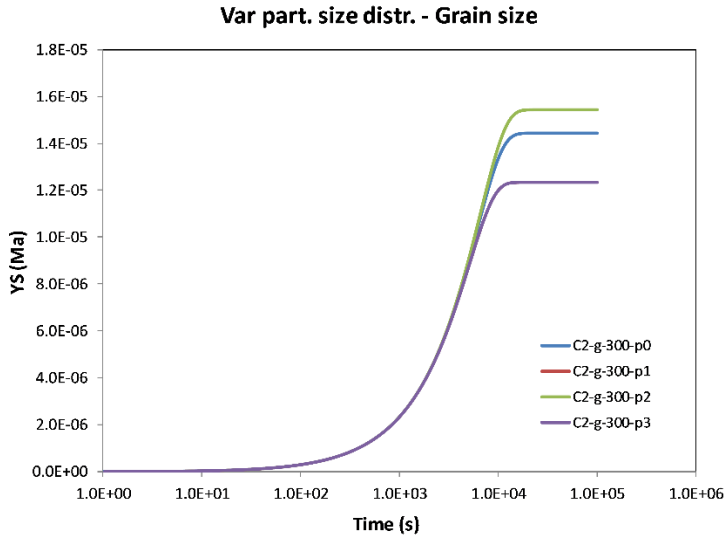

(b)

Figure 5. Generic model calculations showing the effect of differences in size distribution of constituent particles (potential PSN activity) on the softening behavior of an Al-Mn-Fe-Si-alloy cold-rolled to a strain of $\varepsilon = 3$. (a) Kinetics. (b) Evolution in recrystallized grain size.

The effect of varying particle structures, again referring to the C2 alloy and the range of particle structures observed for this alloy, is illustrated in Figure 5. With the rather limited variations present for these alloys, the difference in kinetics is limited (through N_{tot} and N_{PSN} and its effect on the recrystallization kinetics Eq. 11). The most noticeable effect, although still limited is on the final grain size (Figure 5b).

Much more considerable effects may be obtained in the presence of dispersoids, present in the form of high number density and small size. The effect of different scenarios, partially artificially, corresponding to the Zener drag variations given in Figure 6, goes far beyond what has been observed for the relevant C2-alloy. However, some extreme variants are included as they still have relevance for some of the experimental observations made in (Huang, Wang et al. 2014, Huang, Engler et al. 2015, Huang, Li et al. 2015, Huang, Li et al. 2015, Huang and Marthinsen 2015, Huang, Loge et al. 2016, Wang, Huang et al. 2016, Huang, Zhang et al. 2017), in terms of kinetics and final grain structures (slow kinetics and very coarse grains).

Referring to Figure 6, the first 3 variants refer to cases with an increasing Zener drag resulting from pre-existing dispersoids affecting both nucleation of recrystallization and softening kinetics. A case with $P_Z = 0$ is included for reference (dotted line). For the first three cases the effect is most noticeable on the kinetics, and for the third case with $P_Z = 0.2\ MPa$ recrystallization stops before 100% completion because $P_D(t) \leq P_Z$ as a result of significant recovery, and the final stage of softening takes place by "extended" recovery (sub-grain growth and dislocation annihilation) of the remaining deformation structure. In the latter two cases, an even higher Zener drag, acting only during nucleation, has been introduced, the main effect being that nucleation of recrystallization is strongly suppressed and the final grain size can become very large (cf. Eq. 9 and the critical particle size for nucleation $\eta^* \approx \delta^*$ -that goes into Eq. 11).

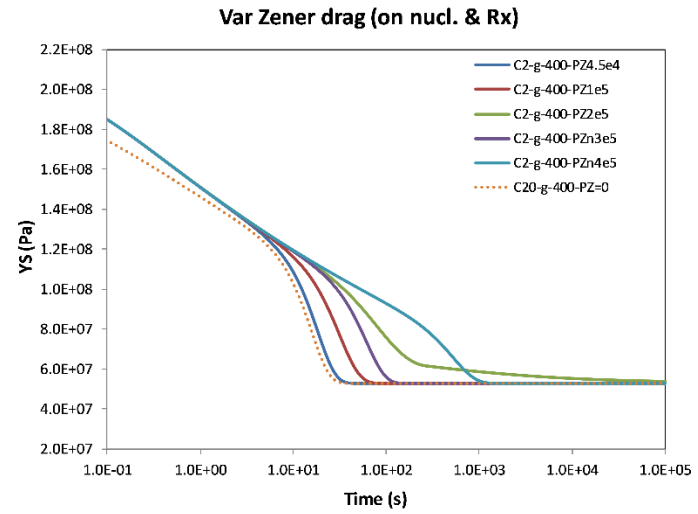

(a)

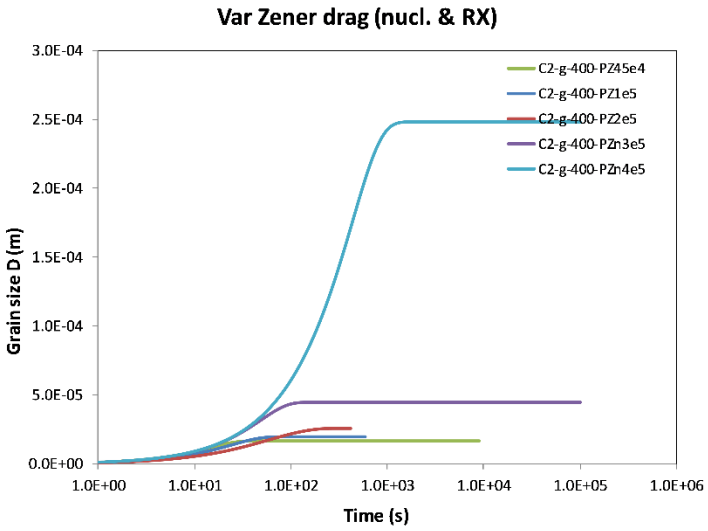

(b)

Figure 6. Generic model calculations showing the effect of differences in Zener drag (Eq. 6), both pre-existing and during annealing, on the softening behavior of an Al-Mn-Fe-Si-alloy cold-rolled to a strain of $\varepsilon = 3$. (a) Kinetics. (b) Evolution in recrystallized grain size. (Note: Zener drag values in legends is given in units of *Pa*).

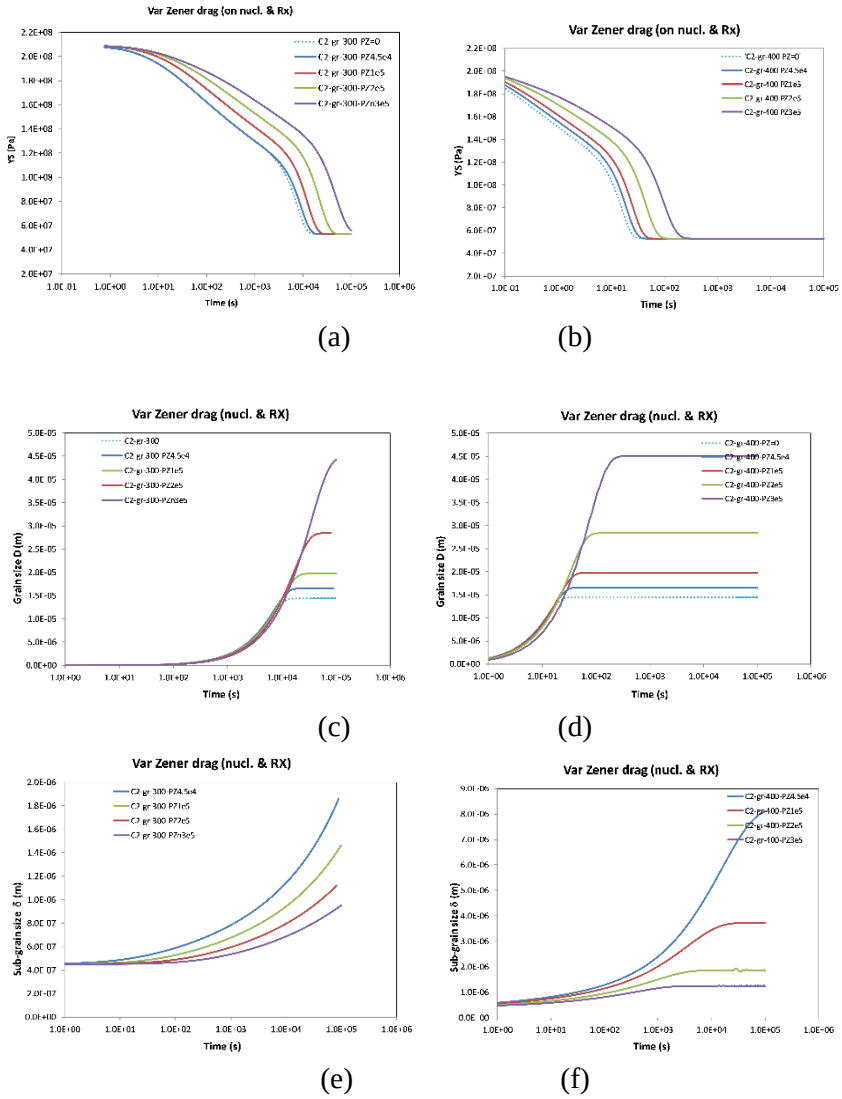

Figure 7. Generic model calculations using a modified sub-grain growth expression (Eq. 8) including Zener-drag effects and its effect, as function of different Zener drag (pre-existing and during annealing), on recovery and its resulting effect on the overall softening behaviour of an Al-Mn-Fe-Si-alloy cold-rolled to a strain of $\varepsilon = 3$. (a) Kinetics, T_{anneal} = 300ºC; (b) Kinetics, T_{anneal} = 400ºC; (c) Evolution in recrystallized grain size, T_{anneal} = 300ºC c) Evolution in recrystallized grain size, T_{anneal} = 400ºC; (e) Sub-grain size evolution during annealing, T_{anneal} = 300ºC; (f) Sub-grain size evolution during annealing, T_{anneal} = 400ºC.

As mentioned in the previous section, as the alloys considered in this work are assumed to be strongly influenced by dispersoids and Zener drag effects, a modified recovery expression for sub-grain growth has been derived (Eq. 8) which also include a possible Zener drag effect on the migration of sub-grain boundaries. Different scenarios are illustrated in Figure 7, referring to two different annealing temperatures and different increasing values of the Zener drag acting both during nucleation of recrystallization and during recovery and recrystallization (i.e., pre-existing dispersoids). The general trend with increasing Zener drag is that recovery is reduced/slowed down and onset of recrystallization delayed, the latter follows from lower nucleation density (suppressed nucleation) as discussed above, which is also indicated by the increasing grain size as shown in Figures 7c and d. The reduced recovery rate is explicitly illustrated by the sub-grain growth curves in Figures 7e. For annealing at 400 ^{o}C we also see that at the highest Zener-drag, sub-grain growth completely stops after a certain time, indicating that the driving force for further sub-grain growth is balanced by the Zener drag, an effect analogous to the Zener-limiting grain size experienced during normal (curvature driven) grain growth in the presence of particles. It is interesting to note that such a Zener-limited sub-grain growth in the context of the *ALSOFT* model has also recently been considered in (Myhr, Furu et al. 2012), however, in their work it was just set as cut-off given by the Zener-limiting sub-grain/grain size (Humphreys and Hatherly 2004).

The above discussion show that recrystallization kinetics is difficult to model for conditions with strong particle drag, it is actually even more challenging if the grain structure after recrystallization needs to be considered, this is illustrated below in Figure 8. The Al-Mn-Fe-Si samples in as-cast states (C1-0) were homogenized at two different conditions to achieve two desired levels of Mn in solid solution (C1-2 and C1-3) and, in turn, different densities of dispersoid particles. It is enough to state that C1-3 has the least Mn in the solid solution while C1-0 has the highest, leading to different precipitation potential. The interested readers are referred to (Huang, Engler et al. 2015) for more details. These three variants were subjected to the same cold rolling process before annealing at different

conditions. The fact that both annealing conditions and microchemistry of the samples have great influence on the recrystallization kinetics and final grain structure can be easily seen in Figure 8. When non-isothermally annealed to 300ºC for 10^5s, recrystallization has completed in C1-3 (see Figure 8g) while it has not initiated for the sample of C1-0 (see Figure 8a). The big difference in grain structure is also obvious when comparing the samples of C1-0 (Figure 8c) and C1-3 (Figure 8i) annealed to 500 ºC.

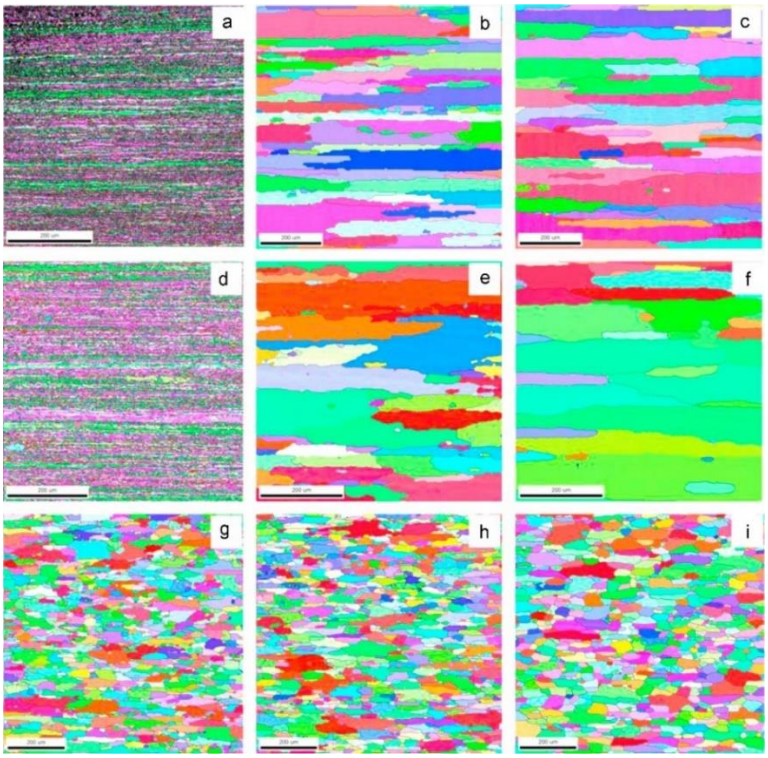

Figure 8. EBSD micrographs showing the effect of microchemistry on the final recrystallized microstructure non-isothermally annealed to different temperatures and hold for 105 s, samples were cold rolled to a strain of 3.0. (a) C1-0, 300 °C@10^5 s; (b) C1-0, 400 °C@10^5 s; (c) C1-0, 500 °C@10^5 s; (d) C1-2, 300 °C@10^5 s; (e) C1-2, 400 °C@10^5 s; (f) C1-2, 500 °C@10^5 s; (g) C1-3, 300 °C@10^5 s; (h) C1-3, 400 °C@10^5 s; (i) C1-3, 500 °C@10^5 s.]. (Huang, Engler et al. 2015).

Recrystallization Kinetics and the Influence of Non-Random Spatial Distribution of Nucleation

As explained above, the *ALSOFT* model is based on the classical Johnson-Mehl-Avrami-Kolmogorov (JMAK) equation (Humphreys and Hatherly 2004), and thus the assumption that the nucleation sites are randomly distributed in space (Kolmogorov 1937, Avrami 1939, Johnson 1939, Avrami 1940, Avrami 1941), i.e.,: $X_V(t) = 1 - \exp(-kt^n)$ (referred to as the JMAK equation), where $X_V(t)$ is the volume fraction of transformed material at the annealing time t, k is a function of growth rate and nucleation rate/density of viable recrystallization nuclei and n the so-called Avrami exponent. In the special case of constant growth rate and a random spatial distribution of nucleation sites, the JMAK equation (1) is exact with $n = 4$ when also the nucleation rate is constant (Johnson-Mehl nucleation kinetics) and $n = 3$ when the nucleation rate decreases so rapidly that all nucleation events effectively occur at the start of recrystallization (site saturated nucleation). The latter is consistent with what is used in the *ALSOFT* model. However, in many cases Avrami exponents of 3 or 4 are not observed, and in general the Avrami exponent varies with time (fraction recrystallized) and typically found to be less than 3 and in some cases even below 2.

It is well known that nucleation of recrystallization is a highly heterogeneous process which typically takes place at deformation heterogeneities like shear bands, transition bands and in deformation zones around large particles (Humphreys 1977). Nevertheless, the assumption of a random spatial distribution of nucleation sites (a prerequisite for the JMAK-equation is often a good assumption, and for an Al-Mg-Mn alloy (AA3004) it has actually been confirmed experimentally that this is an adequate assumption (Daaland and Nes 1996). At the same time computer simulations have shown that both the spatial distribution of nucleation sites and the nucleation rate may influence the transformation kinetics and the recrystallized grain structure in a significant way (Srolovitz, Grest et al. 1988, Furu, Marthinsen et al. 1990, Novikov and Gavrikov 1995,

Marthinsen 1996, Marthinsen and Ryum 1997, Marthinsen, Fridy et al. 1998).

A 3D computer simulation procedure originally developed by Mahin et al (Mahin, Hanson et al. 1980) and later modified to include more general growth rate variations and nucleation models (Marthinsen, Lohne et al. 1989, Saetre, Hunderi et al. 1989) have been used to analyze the influence of various non-random spatial distributions of nucleation sites (Furu, Marthinsen et al. 1990, Marthinsen, Fridy et al. 1998). This is a three-dimensional model in which nuclei are spatially distributed within a cubic volume with periodic boundary conditions start to grow according to a specified nucleation model, and where nucleated grains grow according to a given growth law and the transformation is complete when the grains impinge on one another. The resulting microstructure is analyzed in a two-dimensional section through the cube (similar to most experimental observations), and the model can handle thousands of grains, allowing the kinetics as well as the microstructure evolution (i.e., size distribution of recrystallized grains) to be followed.

Using this 3D simulation procedure, e.g., it was found that with different degrees of spatial clustering of nucleation sites and site saturation nucleation kinetics, that clustering may have a profound effect on both the Avrami exponent n and on the resulting sectioned grain size distributions (Marthinsen, Fridy et al. 1998). Assuming site-saturation nucleation kinetics, the Avrami exponent decreased rapidly from the expected value of 3 with the degree of clustering, and a value of less than 1.5 was observed with a strongly clustered distribution of nucleation sites. Moreover, the size distributions of sectioned grain areas were considerably broadened with clustering as compared to that resulting from randomly distributed nucleation sites. These results illustrate that spatially inhomogeneity of nucleation sites is an important factor that needs to be accounted for when considering recrystallization kinetics and microstructure, and is one factor (amongst several others) which may explain the low (and non-constant) Avrami exponent often observed experimentally.

In heavily deformed commercial aluminum alloys containing large second phase particles, particle stimulated nucleation (PSN) of

recrystallization is often the most important and dominating nucleation mechanism (Humphreys 1977), and the spatial distribution of the large constituent particles is therefore important for the recrystallization behavior. Although the assumption of a near random distribution of particles is fulfilled (Marthinsen, Fridy et al. 1998), exceptions do exist. Marthinsen et al (Marthinsen, Daaland et al. 2003) investigated the spatial distribution of nucleation sites and its effect on the recrystallization kinetics in two commercial Al alloys (commercial purity AA1145, and an Al-Mg-Mn alloy (AA3004) during cold rolling. They documented a transition from a rather non-uniform spatial distribution of particles at low rolling strains, towards a more or less random distribution at high strains.

An important point in this connection is that with a non-random distribution of nucleation sites one of the basic assumptions of the classical JMAK approach (Kolmogorov 1937, Avrami 1939, Johnson 1939, Avrami 1940, Avrami 1941) is no longer valid, and (semi-)analytical modelling based on the JMAK approach of recrystallization (like the *ALSOFT* model) is in general no longer possible. In this case one has to resort to spatially discrete computer simulations, like Potts Monte Carlo models or Cellular Automata models (e.g., (Srolovitz, Grest et al. 1988, Marx, Reher et al. 1999)).

RECOVERY AND RECRYSTALLIZATION BEHAVIOR OF ALMNFESI ALLOYS - A CASE STUDY

In the following, the *ALSOFT* model in its current state and as presented in the modeling section is applied to the experimental results presented in (Huang, Wang et al. 2014, Huang, Engler et al. 2015, Wang, Huang et al. 2016). As far as possible experimentally measured relevant material parameters (e.g., alloy composition, as cast grain size) and microstructure parameters (size and number density of primary particles and dispersoids) have been used as input. Comparisons with experiments and modeling

results are made in terms of the softening behavior (yield stress versus time) and final recrystallized grain size.

The relevant material parameters for the two different alloys considered, i.e., alloy 1 (0.4wt%Mn, 0.5 wt%Fe, 0.15wt%Si) and alloy 2 (1wt% Mn, 0.5 wt% Fe, 0.15wt% Si), only differing in the amount of Mn, as well as the relevant microstructure parameters resulting from the different homogenization treatments (cf. Table 1 below) are given in Table 2 in Appendix. After homogenization both alloys were cold rolled to a strain of $\varepsilon = 1.6$ and $\varepsilon = 3$. In the following these two alloys are denoted C1 and C2, respectively, being consistent with previous literature about these alloys (e.g., (Huang, Wang et al. 2014, Huang, Engler et al. 2015, Wang, Huang et al. 2016)). Here the numerical values for the stored energy, P_D, and Zener drag, P_Z, refer to the initial as-deformed state (or after just a few seconds of initial annealing (5–10 s) for the conditions where the Zener drag mainly originate from concurrent precipitation (cf. (Huang, Wang et al. 2014, Huang, Engler et al. 2015, Wang, Huang et al. 2016)). The actual model parameters used (those that have changed from condition to condition) are given in Table 3 in Appendix. It is noted that for some conditions the *as deformed* structure in terms of sub-grain size and sub-grain interior dislocation density have been adjusted to fit the as deformed yield stress.

Table 1. Four homogenization procedures (including the as-cast condition) and resulting different concentration levels of Mn in solid solution for alloy C2

Sample	Mn_{ss} [wt%]	Dispersoids	Homogenization procedure
C2-0	0.69	Low	As-cast condition
C2-1	0.35	Low	50ºC/h up to 600ºC + 24h@600ºC + quenching
C2-2	0.23	Medium	50ºC/h up to 450ºC + 24h@450ºC + quenching
C2-3	0.21	High	50ºC/h up to 600ºC + 4h@600ºC + 25ºC/h down to 500ºC + 4h@500ºC + quenching

For the conversion of hardness (VHN), as measured experimentally in the previous papers ((Huang, Wang et al. 2014, Huang, Engler et al. 2015, Wang, Huang et al. 2016)) to yield strength (YS) (provided by *ALSOFT*) the following simple relationship has been used:

$$YS(MPa) = 4.5 * VHN - 85 \tag{25}$$

This relationship is consistent with the ones found independently by (Sjølstad, Marthinsen et al. 2004) and (Sande 2011) for similar alloys and conditions.

The resulting experimental yield strength for the different conditions of the C2 alloy (Cf. Table 1 in Appendix) is used as basis to estimate the individual contributions of solid solution strengthening and particle strengthening in Eq. 22. The intrinsic yield stress of the fully soft condition, σ_i, in Eq. 22 is taken to be 10 MPa, a typical value for high purity aluminum alloys.

In order to calculate the particle contribution to the yield stress (Eq. 24) the volume number density N_V is required while the area density N_A is what one obtained from experiments (SEM BSE micrographs) (Wang, Flatoy et al. 2012, Wang, Huang et al. 2016). For the conversion the following formula has been used (Li 2010):

$$N_V = \frac{N_A}{t} \frac{t}{k d_{part} + t} \tag{26}$$

Here d_{part} is the mean particle diameter measured from 2D sections in SEM-BSE images and t is the penetration/information depth taken to be 30 *nm* at a typically used acceleration voltage of 10 kV. The volume fraction of particles (f_p) is then easily calculated, and also the inter-particle spacing, λ, (Eq. 24). When calculating σ_p from Eq. 24 a value of $A = 0.7$ is used and the Taylor factor is set to $M = 3.06$ (the value of random texture) (Brown 1971).

Finally best-fit values of k and c_{ss}^{0} in Eq. 23 are found to be k = 1.95e9 and c_{ss}^{0} = 0.0012.

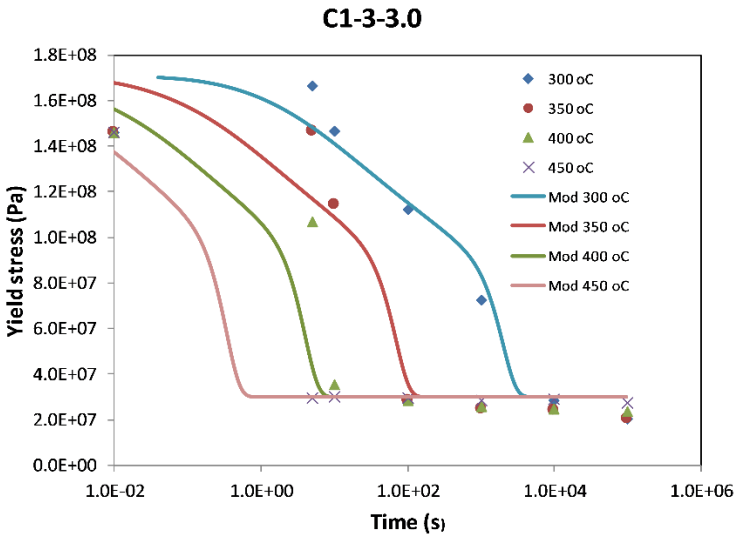

Figure 9. Experimental softening curves and corresponding model predictions for the C1-3 alloy for different annealing temperatures during annealing after cold rolling to a strain of ε = 3.

During softening the value of σ_0 in Eq. 21 is kept constant. In reality due to possible concurrent precipitation, the individual contributions from solid solution (decreasing) and from dispersoids (increasing) may change. However, the two contributions may most probably (at least partly) counterbalance each other, and the effect is therefore for convenience neglected in the present work. The model predictions of the softening behavior of the C1 alloy, together with the corresponding experimental results (corresponding to strain of ε = 3), for homogenization No. 3 (50ºC/h to 600ºC + 4h@600ºC + 25ºC/h to 500ºC + 4h@500ºC + quenching; (Wang, Huang et al. 2016)) is shown in Figure 9 (named C1-3-3; first figure: alloy; second figure: homogenization; third figure: strain (ε = 1.6(2); ε = 3(3)). This homogenization variant is designed to give considerable precipitation (little Mn left in solid solution after

homogenization) and few and fairly large dispersoids, i.e., relatively low Zener drag. Relevant input parameters are given in Table 3 in Appendix. In lack of experimental data for as-deformed sub-grain size and the particle size distribution of constituents (for this particular alloy), similar values as for the C2 alloy for the same homogenization conditions are used. In view of the generic simulations in the previous section with different values of these parameters, this is not believed to represent any significant cause of "error." Although the experimental results are scarce and somewhat scattered the calculated softening curves seems to compare well with the experimental results. The final recrystallized grain size (for all temperatures) is predicted by *ALSOFT* to be D = 14 μm as compared to an experimental value of D = 12 μm.

Changing now to homogenization variant No 2 (50 ºC/h to 450 ºC + 4h@450ºC + quenching) of the C1-alloy after strain of ε = 3 (C1-2-3). Also for this variant most of the Mn precipitate during homogenization (i.e., limited amount of Mn remains in solid solution and thus also limited potential for concurrent precipitation), however in this case a relatively large amount of relatively small pre-existing dispersoids results, giving a static Zener-drag during back-annealing of P_Z = 3x10^4 Pa. The corresponding softening curves are shown in Figure 10.

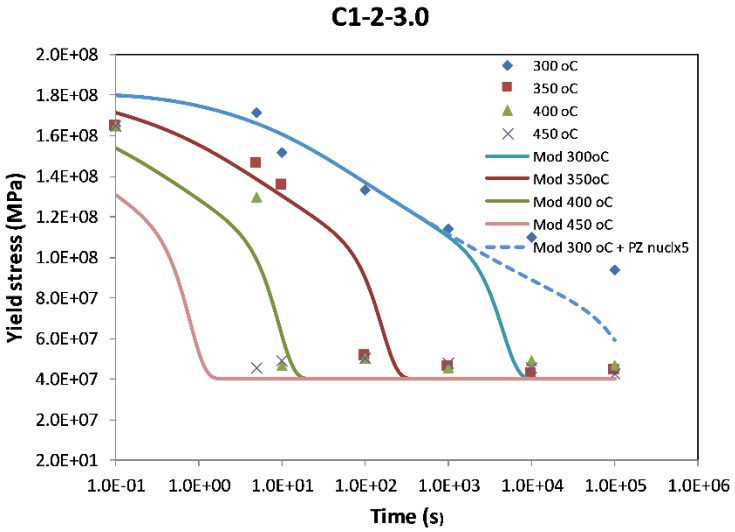

Figure 10. Experimental softening curves and corresponding model predictions for the C1-2 alloy (incl. pre-existing dispersoids) for different annealing temperatures during annealing after cold rolling to a strain of $\varepsilon = 3$.

In this case as well the modeling predictions reproduce the experimental results quite well, except for the lowest temperature where a considerable discrepancy is observed for larger times, where the experimental results show very slow kinetics and a fully soft condition is not reached even after 10^5 s of annealing. However, by a combination of a (un-physical?) much lower mobility pre-factor M_0 (1/10) and a tripled P_Z value a somewhat better agreement may be obtained (dashed line). The predicted grain size is higher than for the first case, i.e., D = 26 μm, however, which also compares reasonably well with experiments, D = 22 μm (cf. Table 2).

We then move to the C2-alloy with the higher amount of Mn (1 wt%). We also start here with homogenization variant No. 3, i.e., the condition with a fairly coarse dispersoid structure and very limited concurrent precipitation. Except for changing the initial sub-grain sizes, in accordance with the experimentally measured values for this alloy at strain of $\varepsilon = 1.6$ and $\varepsilon = 3$ (named C2-3-2 and C2-3-3, respectively), and the Zener drag resulting from the pre-existing dispersoid structure, mainly the same model parameters as for the C1 alloys are used. In addition, two other parameters have been

changed, i.e., $\omega_\delta = 4$ and $C_{PSN} = 0.1$. The modeling results together with the relevant experimental results are shown in Figure 11. Again ignoring a considerable scatter in the experimental results, the model predictions seem for most of the cases quite good. Only at the lower rolling strain (Figure 11a) and the lowest annealing temperature for long annealing times there are some discrepancies.

The experimental and modeled grain sizes are given in Table 2. For the conditions of the largest recrystallized grain size, the grains are quite elongated in the rolling direction. Grain shape is not accounted by the *ALSOFT* model (i.e., only isotropic growth is considered), so the experimental grain sizes given in Table 2, are for comparison the calculated circular area equivalent diameter (ECD). Except for the lowest annealing temperature, the agreement is quite good. At this annealing temperature (T = 300ºC) a better agreement is obtained both for the kinetics and the grain size with a higher pre-existing Zener drag (4x) and lower mobility (0.5x).

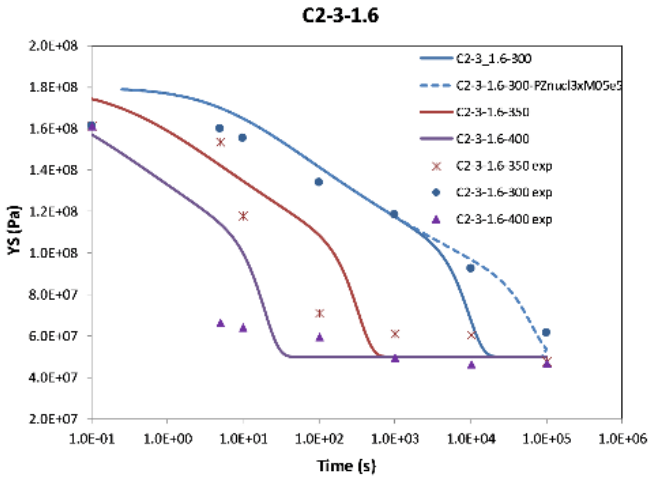

(a)

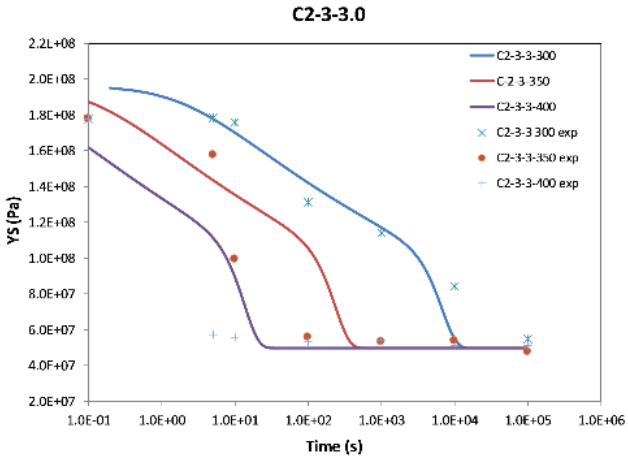

(b)

Figure 11. Experimental softening curves and corresponding model predictions for the C2-3 alloy for different annealing temperatures during annealing after cold rolling to (a) strain of $\varepsilon = 1.6$ and (b) strain of $\varepsilon = 3$.

We now turning to homogenization condition No. 1 (50ºC/h to 600ºC + 24h@600ºC + quenching). In this alloy condition (C2-1) some precipitation has taken place (fairly coarse dispersoid structure), but significant Mn is still left in solution for potential concurrent precipitation during annealing (temperature dependent, see (Huang, Wang et al. 2014) for details). The corresponding modeling results together with relevant experimental results are shown in Figure 12. As shown, again a fairly good agreement is obtained for all conditions. In addition, the experimental and modeled grain sizes correlate quite well, although they are clearly underestimated at the lowest temperature considered (T = 350ºC), i.e., the condition mostly affected by concurrent precipitation. It should be noted however, that to achieve this generally good agreement some modeling parameters needed to be changed (cf. Table 2&3 in Appendix), and some are also changed from condition to condition.

Table 2. Calculated and experimental measured (circle area equivalent diameter) of fully recrystallize grain structures

Alloy/condition	Annealing temperature	Experiment [μm]	Model [μm]	Alt model [μm]
C1-3-3	All	12	14	
C1-2-3	All	22	26	
C2-3-3	450/400/350	24/19/23	19	
C2-3-2	450/400/350	25/23/26	28	
C2-3-2	300	39	28	45
C2-2-3	450	83	88	
C2-2-3	400	77	45	
C2-2-3	350	Na	na	
C2-1-2	450/400	22/20	19	
C2-1-2	350	32	22	
C2-1-3	450/400	19/23	18	
C2-1-3	350	52	21	

Even more difficulties in reproducing the experimental results are experienced for homogenization condition No. 2 (i.e., C2-2; same as for C1-2 alloy), with a large amount of fairly small pre-existing dispersoids (considerable Zener drag acting during both nucleation and growth). Because of this, only a very few selected conditions are shown in Figure 13. The relevant material and model input parameters are given in Tables 1-3 in the Appendix. In particular, it is noted that a considerably higher initial Zener drag (acting during nucleation) need to be included to give reasonable kinetics and grain size, and consistent results were not obtained with the same parameters for all conditions. The annealing behavior at the lower temperatures and for the lower strain was not possible to model with reasonable input parameters and reasonable results.

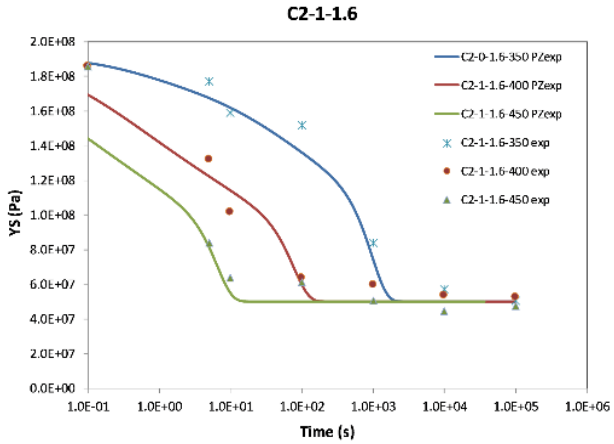

(a)

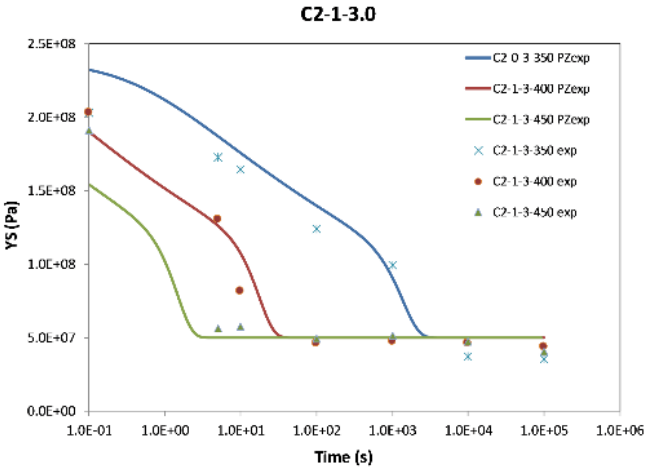

(b)

Figure 12. Experimental softening curves and corresponding model predictions for the C2-1 alloy for different annealing temperatures during annealing after cold rolling to (a) strain of $\varepsilon = 1.6$ and (b) strain of $\varepsilon = 3$.

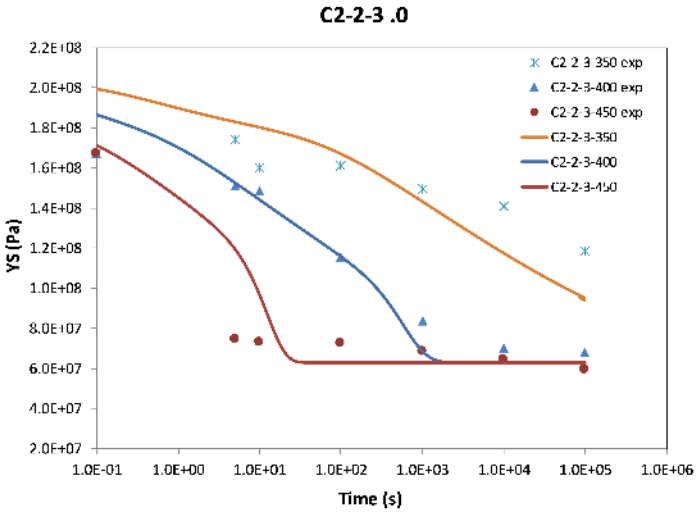

Figure 13. Experimental softening curves and corresponding model predictions for the C2-2 alloy for different annealing temperatures during annealing after cold rolling to a strain of $\varepsilon = 3$.

Attempts to model the softening behavior of the as cast variant C2-0 has not been successful at all. This variant is most strongly influenced by concurrent precipitation and neither the recovery behavior at temperatures and strains where recrystallization is completely supressed nor conditions which do recrystallize but very slowly and with a very coarse fine grain structure, have been possible to model, even with extreme and unphysical values of some of the model parameters.

DISCUSSION

The generic model simulations presented in the first modeling section have clearly shown how and to which extent different material and model parameters influence the softening behavior and final grain structure. Most of the effects are quite easy to understand and in line with what one would expect. However, for certain quantities and model parameters the model dependency are more involved and their influence is not so easy to predict.

For example, the effective solute level (Figure 3) has a quite significant effect on the recovery behavior while the effect on the recrystallization kinetics is less pronounced. Here a lower solute level considerably speeds up the recovery kinetics, which also means that the driving force for recrystallization decreases quite fast, at the same time as the mobility of grain boundaries of actual recrystallized grain increases, with the effects demonstrated in Figure 3. It should be commented that the solute dependency of the mobility (Eq. 19) used here is valid for conditions where solute drag is the rate controlling mechanism for boundary migration and in the limit of a "fully loaded" boundary (Lucke and Stuwe 1971, Hersent, Marthinsen et al. 2013). When the solute concentration, c_{ss}^{eff} , decreases Eq. 19 will eventually break down. In such a case a more sophisticated solute drag model has to be used, which is also valid in the limit of very small solute concentrations, e.g., like the model recently presented by .(Hersent, Marthinsen et al. 2013). In the present work, the problem of a very (too) low effective solute level, is partly avoided by the base level solute parameter c_{ss}^{0} in Eq. 23.

As already mentioned the effective solute concentration is also closely linked to the mobility pre-factor M_0, which has a significant effect on the recrystallization kinetics (Figure 4). In principle this factor, once fitted to one relevant condition, should be kept constant for all conditions and alloys considered (within a certain class of alloys and similar processing conditions). As demonstrated in the previous section (Cf. Table 3 in Appendix) this was not possible in order to get reasonable fit between experiments and model predictions for all conditions in the present work. In particular, for conditions strongly affected by concurrent precipitation, significant changes in the M_0 seemed necessary. This indicates a weakness of the model with possible changes in solute/dispersoid-boundary interaction mechanisms that is not properly accounted for by the model in its present state. In this connection, it should be mentioned that the value of σ_0 in Eq. 21 was kept constant for all simulations in the present work. In reality, especially during conditions of concurrent precipitation, the individual contributions from solid solution (decreasing) and from

dispersoids (increase) may change. However, the two contributions may most probably (at least partly) counterbalance, and the effect is therefore for simplicity neglected in the present work.

The generic model simulations show that several input parameters affect the final grain size, mainly those related to differences in processing conditions (deformation conditions) and the microchemistry state in terms of the size distribution of large constituent particles (potential *PSN* sites) and the size and volume fraction of dispersoids which determines the possible Zener drag operating. A Zener drag resulting from pre-existing dispersoids will, in accordance with general accepted theory (e.g., Humphreys and Hatherly 2004), affect the recrystallization kinetics in two ways, through a reduced effective driving force for recrystallization (Cf. Eq. 18) and through suppressed nucleation due the fact that the critical size for nucleation (Eq. 9) will be increased which again will decrease the density of all three types of nucleation sites (Eq. 13, 14 and 15), see Figure 6. When the Zener drag is large compared with the stored energy P_D, even from the start of annealing, a very coarse grain structure may result, and if it becomes equal to the driving force P_D (continuously decreasing during annealing) recrystallization will stop before completion (cf. Figure 6b). However, if the Zener drag is not acting during nucleation, but results from concurrent precipitation during annealing, the final recrystallized grain size will (according to the model) not be affected, only the kinetics. This is not consistent with most experimental observations in the present and previous work where conditions of strong concurrent precipitation tends to give very coarse-grained structures (Sjolstad, Marthinsen et al. 2004, Tangen, Sjolstad et al. 2010, Huang, Wang et al. 2014, Huang, Engler et al. 2015, Wang, Huang et al. 2016). This observation indicates another weakness of the model, especially for these conditions, which may indicate that the assumption of site saturation nucleation kinetics used presently is not adequate and needs to be relaxed to handle these cases. Attempts to modify the nucleation assumptions of *ALSOFT*, allowing for time-dependent nucleation have recently been reported and promising generic results were shown which were qualitatively in line with typical experimental behaviour (Marthinsen, Friis et al. 2013). It is based on the assumption that nucleation

of recrystallization occurs by a kind of abnormal sub-grain growth mechanism during coarsening of the sub-grain structure during initial stages of annealing, consistent with previous ideas (Holm, Miodownik et al. 2003, Humphreys and Hatherly 2004) and also supported by some recent studies of sub-grain growth in similar alloys (Bunkholt, Marthinsen et al. 2013). Recent detailed experimental investigations of the initial stages of the microstructure evolution in the same alloys as studied here have also indicated time-dependent nucleation of recrystallization (or some kind of incubation time) (Huang, Zhang et al. 2017). The EBSD characterization of early stage of static recrystallization is detailed in Chapter xx of this book.

Since dispersoids and Zener drag effects is quite prominent in the alloys and condition considered, it is also reasonable to assume that Zener drag effects may act during sub-grain growth. Since sub-grain growth is treated analogous to normal grain growth (Furu, Orsund et al. 1995) it is assumed that a Zener drag will act on sub-grain boundaries in a similar way, reducing the effective driving pressure for growth, resulting in the modified sub-grain growth expression in Eq. 8. Its effect on the softening behavior is demonstrated in Figure 7, at two different annealing temperatures. As shown there, the effect is considerable both on the recovery stage and the recrystallization stage, both being increasingly retarded with increasing Zener drag. An important (modeling) effect of this reduced recovery behavior is that the stored energy decreases more slowly, and more seldom P_D becomes less than P_Z and recrystallization stops, which seems to be more consistent with general experimental observations than previous modelling results have indicated, without accounting for the Zener drag effect also during recovery. The recrystallized grain size evolution is shown in Figures 7c and d, and although not related to the different recovery behaviors, the curves illustrate what was also discussed above that a large initial Zener drag (from pre-existing dispersoids) may have a very strong effect on the grain size. The actual sub-grain growth behavior is shown in Figures 7e and f, where Figure 7f illustrates cases where growth is completely stopped when the Zener drag becomes large enough. In all application examples presented in the previous section, the Zener drag modified sub-grain growth equation (Eq. 8) with the appropriate Zener drag values obtained from experiments

(cf. Tables 2&3 in Appendix) have been used with good model predictions indicating this modification to be appropriate.

However, to reproduce both the kinetics and the final grain structure in conditions of significant Zener drag effects it has been necessary to increase the Zener drag acting during nucleation of recrystallization by 2-5 times of its nominal value (cf. Table 3 in Appendix), based on the experimentally measured mean size and number densities of dispersoids and the classical Zener drag expression in Eq. 6. Using more sophisticated expressions for the Zener drag taking into account, e.g., shape factors (Nes, Hunderi et al. 1985) and/or the whole size distribution of dispersoids (Furu and Vatne 2000) change the numerical values of the Zener drag, but is not expected to give changes of the order used in the calculations. Actually using the whole size distribution of dispersoids typically gives lower values for the Zener drag (Furu and Vatne 2000).

An aspect which may influence the value of the Zener drag is sub-grain/grain boundary –particle correlations (Humphreys and Hatherly 2004). Experiments indicate that the precipitation of dispersoids preferentially takes place on grain boundaries and sub-grain boundaries (the latter only relevant for concurrent precipitation). Such correlations may lead to an increased effective Zener drag. By assuming that the sub-grains have a cubic shape with an edge length of δ, and that most of/all the dispersoids (of volume density N_V , radius r and volume fraction f_V) are located at sub grain boundaries, a new equation can be deduced to calculate the Zener drag force (Daaland and Nes 1996, Vatne, Engler et al. 1997). The Zener drag force due to sub-grain boundary dispersoids (where n_A *is the number of dispersoids per unit area of boundary)* can be calculated by

$$P_Z^{SB} = n_A \pi \gamma r = \pi \gamma r N_V \frac{3}{\delta} \tag{27}$$

Using $f_V = {}^{4}\!/_{3}\, \pi r^3 N_V$ to replace N_V, the following expression results

$$P_Z = \frac{\gamma f_V}{4r}\frac{\delta}{r} \tag{28}$$

Comparing with the Zener drag force contributed by randomly distributed dispersoids (Eq. 6),

$$P_Z^{SB} = P_Z^{random}\frac{\delta}{6r} \tag{29}$$

So depending on the ratio $\delta/6r$ the effective Zener drag value may be increased considerably. However, for the present alloys and conditions, the values of the sub-grain and dispersoid sizes are such that this ratio is of the order of 1 for all conditions except the as-cast variant and thus not able to account for the artificially increased model values of P_Z referred to above. If this still were the case, and the cause of suppressed nucleation, this also imply that nucleation of recrystallization cannot be site saturated but takes place after a certain incubation time giving time for (concurrent) precipitation to occur and pin the sub-structure (i.e., some kind of time-dependent nucleation).

On the other hand whether and to which extent classical Zener drag effects operates during recrystallization (i.e., retard boundary migration of a growing recrystallization grain) has recently been questioned (Humphreys and Hatherly 2004, Rollett 2013, Huang, Zhang et al. 2017) in contrast to what most classical literature presents (e.g., Humphreys and Hatherly 2004). The experimental results for the two highest annealing temperatures of the C1 alloy with (C1-2) and without (C1-3) pre-existing dispersoids (Figures 9 and 10) may be in support of such a view as limited or no effects of the pre-existing dispersoids on softening kinetics (although still some effect on the grain structure in terms of shape and size (Huang, Wang et al. 2014) are observed for the C1-2 condition (Figure 8) for these temperatures. On the other hand for the lowest annealing temperature (T = 300ºC) the effect is quite obvious where the condition with pre-existing dispersoids is not even fully recrystallized at 10^5s. Partly recrystallized grain structures caused by

dispersoids is also a well-known phenomenon which supports the classical view. The apparently contradictory observations above for the C1-alloy may indicate a temperature dependent particle drag effect that is not accounted for by the classical temperature independent Zener drag expression. From the very strong dispersoid effect for this alloy and also for several of the other conditions at lower temperatures (Huang, Wang et al. 2014, Huang, Engler et al. 2015, Wang, Huang et al. 2016, Huang, Zhang et al. 2017) one can speculate about a boundary-particle interaction mechanism which involve some kind of thermal activation which give the strong "low temperature" effect while the particle drag effect weakens accordingly at higher temperature. The significant changes of the mobility prefactor M_0 that was needed for a good fit in some of the simulation cases considered above, especially those strongly affected by concurrent precipitation, may be consistent with such an effect, and acted here as a "compensation" for the possible inadequate Zener drag expression for these conditions, or it may possibly be the mobility itself that is actually affected through a shift in migration mechanism.

In the current version of *ALSOFT*, the Zener drag are included by explicitly specifying $P_Z(t)$ on input (i.e., through a weak coupling) where the relevant $P_Z(t)$ evolution may be obtained from experiments or an independent precipitation model. Ideally a fully coupled precipitation and recover/recrystallization model should be used (strong coupling) which in principle account for the effect on precipitation on recovery/ recrystallization (including changes in solid solution level (ignored in the present work) and the possible opposite effect of recovery/recrystallization on the precipitation behavior. Such a coupled model has recently been implemented (Hersent, Huang et al. 2013), based on a recently developed dedicated precipitation model for Al-Mn-Fe-Si-alloys. However, preliminary model predictions by this model indicates a too abrupt precipitation behavior, and a corresponding variation of the Zener drag which gives poor fit to experimental observations, an apparent deficiency which is not unique for this precipitation model.

Thus further work is needed to provide a more adequate precipitation model which may be used in a fully coupled softening model, attempts

towards this direction have been recently summarized in a review paper focusing on the interaction between recrystallization and second-phase particles (Huang, Marthinsen et al. 2018).

[https://linkinghub.elsevier.com/retrieve/pii/S0079642517301287]. It may also need a more sophisticated particle-boundary interaction model capable of predicting the complex behavior discussed in this and related work (Huang, Wang et al. 2014, Huang, Engler et al. 2015, Wang, Huang et al. 2016, Huang, Zhang et al. 2017).

CONCLUSION

In order to describe the influence of microchemistry (solute and second-phase particles in particular) of commercial aluminum alloys on the softening behavior of particle containing alloys, the physical basis and mathematical formulation of the *ALSOFT* model accounting for the combined effect of recovery and recrystallization during back-annealing of heavily deformed aluminium alloys has been reviewed. A modified sub-grain size evolution expression accounting also for a possible Zener drag effect during recovery has been introduced and has proved useful and adequate in model predictions of softening behaviors subjected to particle drag effects.

To demonstrate the different phenomena of recovery and recrystallization and microchemistry interactions, generic model simulations relevant for Al-Mn-Fe-Si-alloys have been performed, which clearly illustrated how and to which extent key material and process parameters affect the softening behavior and the final grain structure. The actual microstructure evolution and associated softening behavior may be significantly affected by a number of material and specific process parameters. However, it is also clearly demonstrated that one of the most pronounced effects is obtained when a strong Zener drag is present already at the onset of recrystallization (i.e., from pre-existing dispersoids and/or dispersoids formed before nucleation of recrystallization take place) causing

strongly suppressed nucleation of recrystallization giving heavily retarded softening kinetics and a very coarse grain structure.

To further illustrate and exemplify the recovery and recrystallization behavior of particle containing commercial aluminum alloys, a set of available softening results for two different Al-Mn-Fe-Si-alloys and processing conditions, giving very different microchemistries in terms of solute and second-phase particle structure have been presented. The experiments clearly demonstrate the strong influence of different microchemistries and in particular the strong dispersoid effects that may be experienced during back-annealing, either from pre-existing dispersoids or concurrent precipitation. The experiments have been accompanied by corresponding model predictions by the *ALSOFT* model, and it has been demonstrated that the model provide quite good predictions, with consistent model parameters, of material and process conditions which experience no or limited influence of pre-existing dispersoids and/or concurrent precipitation. However, providing reasonable model predictions becomes increasingly challenging with increasing influence of dispersoid effects and concurrent precipitation, and for some conditions satisfactory agreement is only obtained with significant and apparently unphysical changes of some model parameters. For the most strongly affected conditions reasonable model predictions were not possible even with extreme changes in the model parameters. The latter observations emphasize that the *ALSOFT* model, and thus also mainly our current understanding of these phenomena and their complex interactions are not fully satisfactory, especially for alloys and conditions strongly affected by dispersoids, either pre-existing and/or as a result of concurrent precipitation.

It is clearly needs for more work and further to improve our understanding and quantitative description (modeling) of these complex phenomena and interactions. An obvious limitation of *ALSOFT* model is the current assumption of site saturated nucleation kinetics, which is not consistent with certain experimental results, and consequently needs to be relaxed. This has been handled by other more recent models (Zurob, Brechet et al. 2006, Dunlop, Brechet et al. 2007, Buken and Kozeschnik 2017), however, although an interesting approach, it is not directly transferrable to

the *ALSOFT* model. The present results and their analysis also seem to indicate that a classical temperature independent Zener drag is not satisfactory to account for the effects observed and that a more sophisticated particle-boundary interaction mechanism may be needed.

APPENDIX

Table 1. Generic *ALSOFT* input (appropriate for C2-0 alloy)

Bitflag for mode selection, currently unused...	as_mode	0
Initial dislocation density (#/m^2)	rho_i	1.98E+13
Initial subgrain size (m)	delta	4.50E-07
Initial recrystallised grain size (m)	r	0
Friction stress (MPa)	R_FLP	5.30E+01
Constant in evolution eq. for dislocation density	B_rho	8.00E+04
Constant in evolution eq. for dislocation density	w_rho	0.5
Constant in evolution eq. for subgrain size	B_delta	2
Constant in evolution eq. for subgrain size	w_delta	5
Constant in expr. for density of particle stimulated	N0	2.67E+17
Constant in particle size distribution (1/m)	L	3.14E+06
Prefactor for mobility (m^4/s)	M0	1.00E+05
Initial (as-cast) grain size (m)	D0	1.00E-04
Constant in evolution eq. for subgrain size	e_delta	0.6667
Constant in evolution eq. for dislocation density	e_rho	0.6667
Constant in strength model	alpha1	0.3
Constant in strength model	alpha2	2.5
Taylor factor	Mtaylor	3
Burgers vector (m)	b	2.86E-10
Debye frequency (1/s)	nu_D	1.00E+13
Grain boundary energy (J/m^2)	gamma_GB	0.3
Constant in expr. for density of particle stimulated	CPE	1.2
Prefactor for density of particle stimulated nucleat	C_PSN	0.2
Constant in expr. for density of grain boundary nucl	C_GB	0.12
Geometric constant in driving pressure for recrystal	alpha	2.5
Missorientation (Deg.)	theta	4

Table 1. (Continued)

Constant for missorientation (Deg.)	theta_c	15
Poisson number	nu	0.33
Initial volume fraction of cube grains	R_c0	0.04
Constant in expr. for density of cube nucleation sit	C_Cube	0.4
Scale factor for mean cube grain size	fCube	1.3
Constant in expr. for volume fraction cube grains	R_cA	2.6
Constant in expr. for volume fraction cube grains	R_cB	1
Constant in expr. for volume fraction cube grains	R_cC	0.3
Constant in expr. for volume fraction cube grains	R_cD	-2
Constant in expr. for volume fraction cube grains	R_cE	0.1
Constant in expr. for volume fraction cube grains	R_cF	-1.4
Constant in expr. for volume fraction cube grains	R_cG	-1.8
Constant in expr. for fraction S deformation texture	R_sA	0.04
Constant in expr. for fraction S deformation texture	R_sB	0.173
Constant in expr. for fraction S deformation texture	R_sC	2
Eff. activation energy for solute diffusion (J/mol)	U_a	2.00E+05
Activation energy for recrystallisation (J/mol)	U_rex	2.00E+05
Prefactor in expr. for shear modulus (Pa) [2.99e10]	G0	2.65E+10
Exp. factor in expr. for shear modulus (K^-1) [5.4e-	G1	0
Temperature during initial deformation (C)	T_def	20
Zener drag during initial deformation (Pa)	PZ_def	0
True strain after initial deformation	strain_def	3
Zener-Holomon parameter (1/s)	Z	4.00E+21
Particle radius [m]	rp	1
Volume fraction particles	fr	0.001

Table 2. Experimental material for data for input to *ALSOFT*

	C2-1	C2-3	C2-0		C2-1		C2-2		C2-3	
Strain ε	3.0	3.0	1.6	3.0	1.6	3.0	1.6	3.0	1.6	3.0
Css (Mn) at%			0.0034		0.0017		0.0011		0.0010	
Css_eff at%	0.0014	0.0014	0.0046		0.0029		0.0023		0.0022	
$\sigma_{ss\text{-}eff}$ (MPa)			53		39		34		33	
N0 (#/m^3)			3.24e17	2.67e17	4.55e16	5.64e16	2.21e17	1.12e17	4.97e16	5.0e16
L (μm)			3.37	3.14	1.78	1.87	3.19	2.78	2.04	2.02
δ (μm)			0.69	0.41	0.98	0.65	0.58	0.46	0.56	0.48
d_part (m)	5.4e-8	1.27e-7						1.05e-7		1.56e-7
N_A (#/m^2)	1.3e12	5.5e10						2.8e12		9.0e11
N_V	1.6e19	2.9e17						2.07e19		4.84e18
Fv	2.51e3	5.9e4						1.26e-2		9.62e-3
λ	1.08e-6	5..4e-6						5.8e-7		1e-6
σ_p (MPa)								16.5		10.2
VHN	55.5	51.4		74.1		64		56.1		57.6
VHN (fully soft)	29	25		33		30		33		30
YS (MPa) (as def)	165	146		248		203		167		174
YS (MPa) (fully soft)	40	30		63.5		50		63.5		50
~ P_D (MPa)	0.75	0.75	0.53	0.92	0.38	0.57	0.64	0.81	0.67	0.78
~ P_Z (MPa)	0.03	0.003	0.14	0.14	0.03	0.03	0.12	0.12	0.075	0.075

Table 3. Actual material and model parameters used in the *ALSOFT* calculations

	C1-3-3	C1-2-3	C1-2-3	C2-3-2	C2-3-2	C2-3-3	C2-1-2	C2-1-2	C2-1-2	C2-1-3	C2-1-3	C2-1-3	C2-2-3	C2-2-3	C2-2-3
T(ºC)	All	All	300	300	>= 350	All	350	400	450	350	400	450	350	400	450
C_{ss}^{eff}	0.0012	0.0014	0.0014	0.0021	0.0021	0.0021	0.0035	0.0035	0.0035	0.0035	0.0035	0.0035	0.0023	0.0023	0.0023
ρ_i	1.6e+13	1.6e+13	1.6e+13	1.5e+13	1.5e+13	1.7e+13	1.6e+13	1.6e+13	1.6e+13	1.6e+13	1.6e+13	1.6e+13	1.6e+13	1.6e+13	1.6e+13
δ (m)	5.0e-07	5.0e-07	5.0e-07	5.5e-07	5.5e-07	4.8e-07	5.0e-07	5.0e-07	5.0e-07	5.0e-07	5.0e-07	5.0e-07	5.0e-07	5.0e-07	5.0e-07
σ_0	3.0e+01	4.0e+01	4.0e+01	5.0e+01	5.0e+01	5.0e+01	5.0e+01	5.0e+01	5.0e+01	5.0e+01	5.0e+01	5.0e+01	6.3e+01	6.3e+01	6.e+01
Bρ	8.0e+04	8.0e+04	8.0e+04	8.0e+04	8.0e+04	8.0e+04	8.0e+04	8.0e+04	8.0e+04	8.0e+04	8.0e+04	8.0e+04	8.0e+04	8.0e+04	8.0e+04
ωρ	0.5	0.5	0.5	0.5	0.5	0.5	0.5	0.5	0.5	0.5	0.5	0.5	0.5	0.5	0.5
Bδ	2	2	2	2	2	2	2	2	2	2	2	2	2	2	2
ωδ	2.5	2.5	2.5	4	4	4	3	4	4	4	5	5	5	5	5
N_0(#/m^3)	5.0e+16	1.12e+17	1.12e+17	4.97e+16	4.97e+16	5.0e+16	4.55e+16	4.55e+16	4.55e+16	5.64e+16	5.64e+16	5.64e+16	1.12e+17	1.12e+17	1.12e+17
L (1/m)	2.02e+06	2.78e+06	2.78e+06	2.04e+06	2.04e+06	2.02e+06	1.78e+06	1.78e+06	1.78e+06	1.87e+06	1.87e+06	1.78e+06	2.78e+06	2.78e+06	2.78e+06
M_0	1.0e+05	1.0e+05	1.0e+05	5.0e+04	1.0e+05	1.0e+05	3.0e+04	1.0e+05	1.0e+05	3.0e+04	3.0e+04	3.0e+04	4.0e+04	2.0e+04	4.0e+04
D_0	1.0e-04	1.0e-04	1.0e-04	1.0e-04	1.0e-04	1.0e-04	1.0e-04	1.0e-04	1.0e-04	1.0e-04	1.0e-04	1.0e-04	1.0e-04	1.0e-04	1.0e-04
CPE	1.2	1.2	1.2	1.2	1.2	1.2	1.2	1.2	1.2	1.2	1.2	1.2	1.2	1.2	1.2
C_{PSN}	0.2	0.2	0.2	0.1	0.1	0.1	0.1	0.1	0.1	0.1	0.1	0.1	0.1	0.1	0.1
C_{GB}	0.12	0.12	0.12	0.12	0.12	0.12	0.12	0.12	0.12	0.12	0.12	0.12	0.12	0.12	0.12
P_Z (Pa)	3.0e+00	3.0e+04	3.0e+04	2.5e+05	7.5e+04	7.5e+04	1.0e+05	3.0e+04	3.0e+04	1.0e+05	3.0e+04	3.0e+04	5.0e05	5.0e+05	5.0e+05
ε	3.0	3.0	3.0	1.6	1.6	3.0	1.6	1.6	1.6	3.0	3.0	3.0	3.0	3.0	3.0

REFERENCES

Alvi, M. (2005). Recrystallization kinetics and microstructural evolution in hot rolled aluminum alloys. Pittsburgh, US, Carnegie Mellon University.

Alvi, M. H., S. W. Cheong, J. P. Suni, H. Weiland and A. D. Rollett (2008). "Cube texture in hot-rolled aluminum alloy 1050 (AA1050) - nucleation and growth behavior." *Acta Materialia* **56**(13): 3098-3108.

Avrami, M. (1939). "Kinetics of phase change I. General Theory." *Journal of Chemical Physics* **7**: 1103-1112.

Avrami, M. (1940). "Kinetics of Phase Change. II Transformation-Time Relations for Random Distribution of Nuclei." *The Journal of Chemical Physics* **8**: 212-224.

Avrami, M. (1941). "Granulation, Phase Change, and Microstructure Kinetics of Phase Change. III." *The Journal of Chemical Physics* **9**: 177-184.

Brown, L. M., Ham, R. K. (1971). *Strengthening Methods in Crystals*. Amsterdam, Elsevier.

Buken, H. and E. Kozeschnik (2017). "A Model for Static Recrystallization with Simultaneous Precipitation and Solute Drag." *Metallurgical and Materials Transactions a-Physical Metallurgy and Materials Science* **48A**(6): 2812-2818.

Bunkholt, S., K. Marthinsen and E. Nes (2013). Recovery Kinetics in High Purity and Commercial Purity Aluminium Alloys. *Recrystallization and Grain Growth V. M. Barnett*. **753:** 235-238.

Cahn, J. W. (1962). "Impurity-drag effect in grain boundary motion." *Acta Metallurgica* **10**(SEP): 789-&.

Daaland, O. and E. Nes (1996). "Origin of cube texture during hot rolling of commercial Al-Mn-Mg alloys." *Acta Materialia* **44**(4): 1389-1411.

Daaland, O. and E. Nes (1996). "Recrystallization texture development in commercial Al-Mn-Mg alloys." *Acta Materialia* **44**(4): 1413-1435.

Dunlop, J. W. C., Y. J. M. Brechet, L. Legras and H. S. Zurob (2007). "Modelling isothermal and non-isothermal recrystallisation kinetics:

Application to Zircaloy-4." *Journal of Nuclear Materials* **366**(1-2): 178-186.

Engler, O., L. Lochte and J. Hirsch (2007). "Through-process simulation of texture and properties during the thermomechanical processing of aluminum sheets." *Acta Materialia* **55**(16): 5449-5463.

Furu, T., K. Marthinsen and E. Nes (1990). "Modeling recrystallization." *Materials Science and Technology* **6**(11): 1093-1102.

Furu, T., R. Orsund and E. Nes (1995). "Subgrain growth in heavily deformed aluminum - experimental investigation and modeling treatment." *Acta Metallurgica Et Materialia* **43**(6): 2209-2232.

Furu, T. and H. E. Vatne (2000). Grain structure control of flat extruded AA6082 alloy. *Aluminum Alloys: Their Physical and Mechanical Properties*, Pts 1-3. E. A. Starke, T. H. Sanders and W. A. Cassada. **331-3:** 843-848.

Hersent, E., K. Huang, J. Friis and K. Marthinsen (2013). Modeling the evolution in microchemistry and its effects on the softening behavior of cold rolled AlFeMnSi-alloys during annealing. *Recrystallization and Grain Growth* V. M. Barnett. **753:** 143-+.

Hersent, E., K. Marthinsen and E. Nes (2013). "The Effect of Solute Atoms on Grain Boundary Migration: A Solute Pinning Approach." *Metallurgical and Materials Transactions a-Physical Metallurgy and Materials Science* **44A**(7): 3364-3375.

Holm, E. A., M. A. Miodownik and A. D. Rollett (2003). "On abnormal subgrain growth and the origin of recrystallization nuclei." *Acta Materialia* **51**(9): 2701-2716.

Huang, K., O. Engler, Y. J. Li and K. Marthinsen (2015). "Evolution in microstructure and properties during non-isothermal annealing of a cold-rolled Al-Mn-Fe-Si alloy with different microchemistry states." *Materials Science and Engineering a-Structural Materials Properties Microstructure and Processing* **628**: 216-229.

Huang, K., Y. J. Li and K. Marthinsen (2015). "Effect of heterogeneously distributed pre-existing dispersoids on the recrystallization behavior of a cold-rolled Al-Mn-Fe-Si alloy." *Materials Characterization* **102**: 92-97.

Huang, K., Y. J. Li and K. Marthinsen (2015). "Factors affecting the strength of P{011}<566 >-texture after annealing of a cold-rolled Al-Mn-Fe-Si alloy." *Journal of Materials Science* **50**(14): 5091-5103.

Huang, K., R. E. Loge and K. Marthinsen (2016). "On the sluggish recrystallization of a cold-rolled Al-Mn-Fe-Si alloy." *Journal of Materials Science* **51**(3): 1632-1643.

Huang, K. and K. Marthinsen (2015). "The effect of heating rate on the softening behavior of a deformed Al-Mn alloy with strong and weak concurrent precipitation." *Materials Characterization* **110**: 215-221.

Huang, K., K. Marthinsen, Q. L. Zhao and R. E. Loge (2018). "The double-edge effect of second-phase particles on the recrystallization behavior and associated mechanical properties of metallic materials." *Progress in Materials Science* **92**: 284-359.

Huang, K., N. Wang, Y. J. Li and K. Marthinsen (2014). "The influence of microchemistry on the softening behavior of two cold-rolled Al-Mn-Fe-Si alloys." *Materials Science and Engineering a-Structural Materials Properties Microstructure and Processing* **601**: 86-96.

Huang, K., K. Zhang, K. Marthinsen and R. E. Loge (2017). "Controlling grain structure and texture in Al-Mn from the competition between precipitation and recrystallization." *Acta Materialia* **141**: 360-373.

Humphreys, F. J. (1977). "Nucleation of recrystallization at 2nd phase particles in deformed aluminum." *Acta Metallurgica* **25**(11): 1323-1344.

Humphreys, F. J. and M. Hatherly (2004). Recrystallization and related annealing phenomena. Amsterdam, Elsevier.

Johnson, W. A., Mehl, R. F. (1939). "Reaction Kinetics in Processes of Nucleation and Growth." *Trans. Metall. Soc. AIME* **135**.

Kolmogorov, A. N. (1937). "On the statistical theory of metal crystallization." Izv. Akad. Nauk. USSR-Ser Matemat **1**: 355-359.

Li, Y. (2010). Methods for quantitative measurement of dispersoids in Nonheat-treatable aluminum alloys. Trondheim, Norway, SINTEF.

Lucke, K. and H. P. Stuwe (1971). "Theory of impurity controlled grain boundary motion." *Acta Metallurgica* **19**(10): 1087-&.

Mahin, K. W., K. Hanson and J. W. Morris (1980). "Comparative-analysis of cellular and Johnson-Mehl microstructures through computer-simulation." *Acta Metallurgica* **28**(4): 443-453.

Marthinsen, K. (1996). "Repeated grain boundary and grain corner nucleated recrystallization in one- and two-dimensional grain structures." *Modeling and Simulation in Materials Science and Engineering* **4**(1): 87-100.

Marthinsen, K., Abtahi, S., Sjølstad, K., Holmedal, B., Nes, E., Johansen, A., Sæter, J. A., Furu, T., Engler, O., Lok, Z. J., Talamantes-Silva, J., Allen, C., Liu, C. (2004). "*Modelling the Evolution of Microstructure and Mechanical Properties during Processing of AA3103*." Alumnum **80**: 729-738.

Marthinsen, K., O. Daaland, T. Furu and E. Nes (2003). "The spatial distribution of nucleation sites and its effect on recrystallization kinetics in commercial aluminum alloys." *Metallurgical and Materials Transactions a-Physical Metallurgy and Materials Science* **34A**(12): 2705-2715.

Marthinsen, K., J. M. Fridy, T. N. Rouns, K. B. Lippert and E. Nes (1998). "Characterization of 3-D particle distributions and effects on recrystallization kinetics and microstructure." *Scripta Materialia* **39**(9): 1177-1183.

Marthinsen, K., J. Friis and O. Engler (2013). Modeling time-dependent nucleation of recrystallization in aluminum alloys. *Recrystallization and Grain Growth* V. M. Barnett. **753:** 147-152.

Marthinsen, K., J. Friis, B. Holmedal, I. Skauvik and T. Furu (2012). Modeling the recrystallization behavior during industrial processing of aluminum alloys. *Recrystallization and Grain Growth* Iv. E. J. Palmiere and B. P. Wynne. **715-716:** 543-548.

Marthinsen, K., O. Lohne and E. Nes (1989). "The development of recrystallization microstructures studied experimentally and by computer simulation." *Acta Metallurgica* **37**(1): 135-145.

Marthinsen, K. and E. Nes (2001). "Modelling strain hardening and steady state deformation of Al-Mg alloys." *Materials Science and Technology* **17**(4): 376-388.

Marthinsen, K. and N. Ryum (1997). "Transformation kinetics and microstructure for grain boundary nucleated recrystallization in two dimensions." *Acta Materialia* **45**(3): 1127-1136.

Marx, V., F. R. Reher and G. Gottstein (1999). "Simulation of primary recrystallization using a modified three-dimensional cellular automaton." *Acta Materialia* **47**(4): 1219-1230.

Myhr, O. R., Furu, T., Emmerhoff, J., Skauvik, I., Engler, O. (2012). Through Process Modelling (TPM) of Grain Structure Evolution in 6xxx Series Aluminum Extrusions. !0th International Aluminium Extrusion Technology Seminar and Exposition, Miami, Florida, US.

Nes, E. (1995). "Constitutive laws for steady-state deformation of metals, a microstructural model." *Scripta Metallurgica Et Materialia* **33**(2): 225-231.

Nes, E. (1995). "Recovery revisited." *Acta Metallurgica Et Materialia* **43**(6): 2189-2207.

Nes, E. (1997). "Modelling of work hardening and stress saturation in FCC metals." *Progress in Materials Science* **41**(3): 129-193.

Nes, E. and J. D. Embury (1975). "Influence of a fine particle dispersion on recrystallization behavior of a 2-phase aluminum-alloy." *Zeitschrift Fur Metallkunde* **66**(10): 589-593.

Nes, E. and K. Marthinsen (2002). "Modeling the evolution in microstructure and properties during plastic deformation of f.c.c.-metals and alloys - an approach towards a unified model." *Materials Science and Engineering a-Structural Materials Properties Microstructure and Processing* **322**(1-2): 176-193.

Nes, E., N. Ryum and O. Hunderi (1985). "On the Zener drag." *Acta Metallurgica* **33**(1): 11-22.

Novikov, V. Y. and I. S. Gavrikov (1995). "Influence of heterogeneous nucleation on microstructure and kinetics of primary recrystallization." *Acta Metallurgica Et Materialia* **43**(3): 973-976.

Read, W. T. (1953). *Dislocations in Crystals*. New York, Mcgraw-Hill.

Rollett, A. D. (2013). Personal communications.

Saeter, J. A., Forbord, B, Vatne, H. E., Nes, E. (1998). Modeling recovery and recrystallization, applied to back-annealing of aluminum sheet

alloys. *Proceedings of the 6th International Conference on Aluminum Alloys* (ICAA6), Japan, Japanese Institute of Light Metals (JILM).

Saetre, T. O., O. Hunderi and N. Ryum (1989). "Modeling grain-growth in 2 dimensions." *Acta Metallurgica* **37**(5): 1381-1387.

Sande, G. (2011). *Numerical modeling of recrystallization in aluminum alloys*. Trondheim, Norway, Norwegian University of Science and Technology.

Sjolstad, A., K. Marthinsen and E. Nes (2004). Modeling the softening behavior of commercial AlMn-alloys. *Recrystallization and Grain Growth*, Pts 1 and 2. B. Bacroix, J. H. Driver, R. LeGall et al. **467-470:** 677-682.

Srolovitz, D. J., G. S. Grest, M. P. Anderson and A. D. Rollett (1988). "Computer-simulation of recrystallization. 2. Heterogeneous nucleation and growth." *Acta Metallurgica* **36**(8): 2115-2128.

Tangen, S., K. Sjolstad, T. Furu and E. Nes (2010). "Effect of Concurrent Precipitation on Recrystallization and Evolution of the P-Texture Component in a Commercial Al-Mn Alloy." *Metallurgical and Materials Transactions a-Physical Metallurgy and Materials Science* **41A**(11): 2970-2983.

Vatne, H. E. (1999). *Modelling of Metal Rolling Processes* 3. London, IOM Communications.

Vatne, H. E., O. Engler and E. Nes (1997). "Influence of particles on recrystallisation textures and microstructures of aluminum alloy 3103." *Materials Science and Technology* **13**(2): 93-102.

Vatne, H. E., T. Furu, R. Orsund and E. Nes (1996). "Modeling recrystallization after hot deformation of aluminum." *Acta Materialia* **44**(11): 4463-4473.

Vatne, H. E., K. Marthinsen, R. Orsund and E. Nes (1996). "Modeling recrystallization kinetics, grain sizes, and textures during multi-pass hot rolling." *Metallurgical and Materials Transactions a-Physical Metallurgy and Materials Science* **27**(12): 4133-4144.

Wang, N., J. E. Flatoy, Y. J. Li and K. Marthinsen (2012). "Evolution in microchemistry and its effects on deformation and annealing behaviour

of an AlMnFeSi alloy." *Proceedings of the 13th International Conference on Aluminum Alloys* (Icaa13): 1837-1842.

Wang, N., K. Huang, Y. J. Li and K. Marthinsen (2016). "The Influence of Processing Conditions on Microchemistry and the Softening Behavior of Cold Rolled Al-Mn-Fe-Si Alloys." *Metals* **6**(3).

Zurob, H. S., Y. Brechet and J. Dunlop (2006). "Quantitative criterion for recrystallization nucleation in single-phase alloys: Prediction of critical strains and incubation times." A*cta Materialia* **54**(15): 3983-3990.

LCH